Molecular Catalysis 492 (2020) 110917

Contents lists available at ScienceDirect

Molecular Catalysis

journal homepage: www.elsevier.com/locate/mcat

Selective aerobic oxidation of benzyl alcohol on alumina supported Au-Ru and Au-Ir catalysts

G. Nagy[a,*], T. Gál[a], D.F. Srankó[a], G. Sáfrán[b], B. Maróti[c], I.E. Sajó[d], F.-P. Schmidt[e,f], A. Beck[a]

[a] Centre for Energy Research, Surface Chemistry and Catalysis Department, PO Box 49, H-1525 Budapest, Hungary
[b] Centre for Energy Research, Institute for Technical Physics and Materials Science, PO Box 49, H-1525 Budapest, Hungary
[c] Centre for Energy Research, Nuclear Analysis and Radiography Department, PO Box 49, H-1525 Budapest, Hungary
[d] University of Pécs, Szentágothai Research Centre, Ifjúság Street 20, H-7624 Pécs, Hungary
[e] Institute of Physics, University of Graz, Universitätsplatz 5, 8010 Graz, Austria
[f] Institute for Electron Microscopy and Nanoanalysis, Graz University of Technology, Steyrergasse 17, 8010 Graz, Austria

ARTICLE INFO

Keywords:
Benzyl alcohol oxidation
Gold
Ruthenium
Iridium
CO-DRIFTS

ABSTRACT

Selective oxidation of benzyl alcohol to benzaldehyde with molecular oxygen was studied over sol-derived alumina supported bimetallic Au-Ru and Au-Ir (nominal atomic ratio 1:1) with respect to Au, Ru and Ir monometallic catalysts in both calcined and subsequently reduced states with and without equimolar K_2CO_3 in toluene at 80 °C. The Au and after an induction period also Au-Ru and Au-Ir samples had good activity and selectivity in the presence of K_2CO_3, the monometallic Ir and Ru ones showed negligible activity. The different pretreatments did not cause large difference in the catalytic performance, except the Ir containing samples, which were more active in reduced state.

The samples were characterized by TEM, STEM-EDS, UV-Vis spectroscopy, XRD and TPR. The surface of the catalysts was investigated by XPS and CO adsorption followed by infrared spectroscopy. We confirmed the interaction between Au and both second metals, and a strongly decreased CO adsorption on gold in the bimetallic samples compared to the monometallic one. Based on the reaction rates related to the estimated Au and second metal surfaces in the bimetallic and corresponding monometallic catalysts synergetic effect is suggested for the calcined and reduced Au-Ru and reduced Au-Ir catalysts in reaction with base addition.

1. Introduction

One of the prime requirements of a sustainable world is the development of "green" ways for the production of commodity products. Nowadays the industry still uses conventional and very harmful stoichiometric oxidizing reagents (such as nitric acid and metal oxides) to produce fine chemicals. Furthermore, these processes also produce huge amounts of waste. The oxidizing agents could be substituted with air or molecular oxygen by using the appropriate catalysts. Since Haruta discovered the catalytic activity of the nano-sized gold particles in low temperature CO oxidation [1], its applications widened, and gold has become a well-known catalyst also for selective oxidations of various substrates. Supported gold-based catalysts have been investigated in a lot of oxidation reactions for example: aliphatic alcohol [2–4], aromatic alcohol [2,5,6] and sugars [7–9] oxidation. In the case of benzyl alcohol oxidation to benzaldehyde, the over oxidation of the substrate is a problem (Scheme 1). This reaction has two typical by-products; benzoic acid and benzyl benzoate. Benzoic acid is a very strong inhibitor of gold catalysts [10–13]. Skupien and co-workers made a profound study about the poison effect of benzoic acid [13]. They showed that benzoic acid can strongly inhibit the reaction at a very low concentration (near or under detection limit). Benzoic acid can react with the unconverted benzyl alcohol and this reaction could produce the benzyl benzoate [14]. However, Skupien and co-workers showed that under base conditions the benzyl benzoate is formed dominantly in the reaction of benzyl alcohol and benzaldehyde [13].

Using a second metal to improve the stability, selectivity and activity of the catalysts is a well-known method. There are many studies about application of gold containing bimetallic systems in oxidation of benzyl alcohol. For example Li and co-workers have found a synergistic effect of Au-Pd/MgO catalyst in toluene (two different preparation methods were used where ~80 and ~250 % increase in catalytic activity was observed compared to the corresponding monometallic gold catalysts and the selectivity was ~100 % in both cases) [15]. Lu and co-workers examined P123 stabilized Au-Ag colloids without support and high improvement was observed compared to the monometallic Au and Ag colloid (catalytic activity increased from TOF = 53 h^{-1} to 216 h^{-1}) [16]. Silica supported Au-Ag

* Corresponding author.
E-mail address: nagy.gergely@energia.mta.hu (G. Nagy).

https://doi.org/10.1016/j.mcat.2020.110917
Received 7 December 2019; Received in revised form 14 February 2020; Accepted 22 March 2020
Available online 15 May 2020

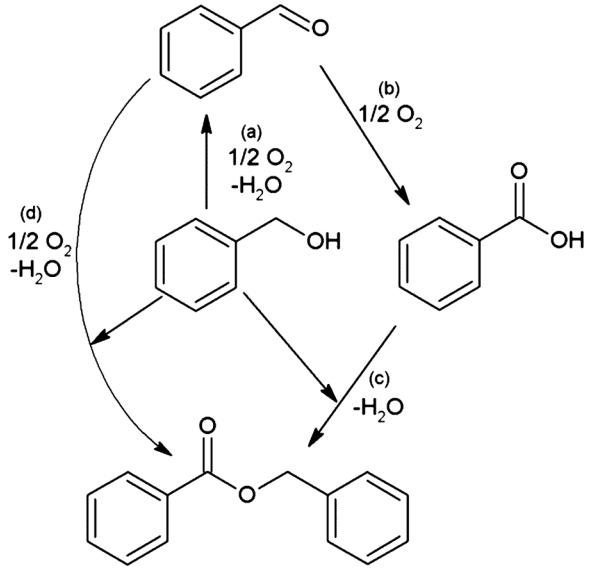

Scheme 1. Oxidation of benzyl alcohol (a) oxidation of benzyl alcohol to benzaldehyde; (b) oxidation of benzaldehyde to benzoic acid (c) esterification of benzyl alcohol and benzoic acid and (d) esterification of benzyl alcohol and benzaldehyde under oxidative conditions to benzyl benzoate.

colloids of various Au/Ag molar ratio also presented synergistic effect at low Ag/Au ratio [17].

In several articles it has already been reported that the performance of Au nanoparticles could be improved by Ru in CO oxidation [18], partial (to $CO+H_2$) and complete oxidation of methanol [19,20] and selective oxidation of n-octanol and glycerol [21,22]. Furthermore it has already been shown that ruthenium alone [23–29] can catalyse the oxidation of aromatic alcohols, where the active form of ruthenium is $Ru(OH)_x$ or hydrated RuO_2, which deactivates on complete dehydration. The most active $Ru(OH)_x$ acts as a bifunctional (Lewis acid Ru cations and Brönsted base OH) catalyst [30]. In these works no base was added to the catalytic reaction and no deactivation was observed, but the substrate/metal ratio was quite low ($S/M < 125$). It is to be noted that for recycling of the catalysts washing with NaOH solution was applied to regenerate the catalyst. On the other side fast and reversible benzoic acid inhibition was observed in continuous flow reactor [31].

Iridium can be used to improve the activity and the stability of gold, such as in the oxidation of CO [32–34], total oxidation of propene [35] and toluene [36] assisting in the oxygen activation at lower temperatures, or in the selective hydrogenation of cinnamaldehyde [37]. Ir complexes were reported to be efficient catalysts in oxidative dehydrogenation of alcohols [38].

According to these literature results the Au-Ru and Au-Ir seemed to be promising bimetallic compositions and to the best of our knowledge, other researchers have not examined yet these two systems in the oxidation of benzyl alcohol.

In this work alumina supported gold-ruthenium and gold-iridium samples were prepared by adsorption of bimetallic, polyvinyl alcohol (PVA) stabilized Au-Ru and Au-Ir sols, and tested after calcination (for removal of organic residues) and also subsequent reduction in benzyl alcohol oxidation with respect to the corresponding monometallic catalysts. The effect of the Ru and Ir introduction on the gold catalyst and the addition of K_2CO_3 in liquid phase oxidation of benzyl alcohol were investigated in relation with the catalysts structure.

2. Experimental

2.1. Materials

The catalysts were prepared by using $HAuCl_4.3H_2O$ (Aldrich); $RuCl_3{\cdot}xH_2O$ (Aldrich); $(NH_4)_2IrCl_6$ (Ventron); PVA (Sigma); $NaBH_4$ (Ventron); commercial alumina (Degussa Aluminiumoxid C) and purified water (Milli-Q). Toluene (Fisher); benzyl alcohol (Lach-ner); K_2CO_3 (Lach-ner) were used in the catalytic reactions and dodecane (Fisher) was the internal reference for GC analysis.

2.2. Preparation of catalysts

Firstly, the monometallic (Au, Ru) and bimetallic (Au-Ru, Au-Ir) sols were prepared by reduction and co-reduction, respectively, with $NaBH_4$ in presence of a stabilizer (PVA) using 5.3 mM $HAuCl_4$, 6.0 mM $RuCl_3$ and 8.9 mM $(NH_4)_2IrCl_6$ precursor stock solutions. 164 μmol metal ions (in case of bimetallic 82 μmol $HAuCl_4$ and 82 μmol $RuCl_3$ or $(NH_4)_2IrCl_6$) containing solutions and 30 mL 0.2 wt% PVA were mixed, and diluted to 500 mL with Milli-Q water (resistivity: 18.2 MΩ cm at 25 °C). The solutions were cooled and stirred in a cooling bath of ice and water. 47 mg of $NaBH_4$ (1.24 mmol) was dissolved in 50 mL of Milli-Q water and then it was suddenly added to the metal precursor solutions under stirring. The reductions were indicated by sudden change of colour. In case of the monometallic Au and the bimetallic Au-Ru and Au-Ir the originally light yellow, light brownish red and light brownish yellow solutions turned to dark brownish red, dark grey, and dark red, respectively. The monometallic Ru precursor solution turned from light brown via momentary decolouration to greenish brown. The sols of Au, Ru, Au-Ru, Au-Ir were adsorbed on appropriate amount of Al_2O_3 nano powder to provide the nominal metal loadings of 90 μmol/g_{cat} (45 μmol/g_{cat} Au and 45 μmol/g_{cat} Ru or Ir in the bimetallic samples). All suspensions were filtered and washed with 300 mL of Milli-Q water. The pellets were dried overnight at 80 °C. Before the catalytic tests the alumina supported catalysts were calcined in synthetic air flow (100 mL/min) at 400 °C for 1 h ("calc" samples) to remove the PVA residues. Reduced form of the catalysts ("red" samples) were also studied after the treatment of the calcined samples in hydrogen flow (100 mL/min) for 30 min at 350 °C in the case of Au/Al_2O_3 and at 400 °C in the case of Ru/Al_2O_3, $Au\text{-}Ru/Al_2O_3$ and $AuIr/Al_2O_3$.

The Ir/Al_2O_3 was prepared by wet impregnation technique. 13 mL of 8.9 mM $(NH_4)_2IrCl_6$ acidified with HCl to pH = 1.5 was added to 600 mg of alumina nanopowder, then under continuous stirring heated gradually to 80 °C in 90 min and evaporated the water in about additional 90 min. The dry sample was kept in a drying furnace at 80 °C for a night. In the last step it was calcined at 400 °C for 1 h ("calc" sample). The colour of the sample changed from purple grey to bluish grey. For several measurements consecutive reduction was applied at 400 °C for 30 min ("red" sample).

2.3. Sample characterization

The actual metal content of the samples was determined by non-destructive nuclear elemental analysis techniques, with **prompt-gamma neutron** activation analysis (PGAA) in case of Au/Al_2O_3 and $AuRu/Al_2O_3$ [39] and with **in-beam neutron activation analysis (IB-NAA)** [40] in case of the Ir containing samples at the PGAA facility of the Budapest Neutron Centre. The samples (460 − 600 mg) were irradiated in a guided neutron beam for about 18 h and the gamma-rays were detected. After the measurement, when the radiation of the catalyst decreased to the required level the samples could be used for other experiments.

Transmission electron microscopy investigations were carried out on the calcined and reduced form of the various samples drop dried on a carbon coated Cu micro grid with a JEOL 3010 microscope operating at 300 kV with a point resolution of 0.17 nm. The average diameters of the Au/Ru/Ir containing nanoparticles (NPs) were determined by the analysis of about 200 particles.

Scanning transmission electron microscopy (STEM) measurements in combination with energy dispersive x-ray spectroscopy (EDS) were carried out as follows. The Au-Ru sol drop dried on a carbon

coated copper micro grid was investigated in a probe-corrected FEI Titan G2 60 – 300 microscope at 300 kV, equipped with a high-brightness Schottky field emission source (X-FEG) and a SuperX EDX detection system. A 19.6 mrad convergence semi-angle was used. EDX spectra were recorded using the spectrum imaging method, where the focused electron beam was scanned across the region of interest with a step size ranging from 0.1 to 0.15 nm. The Au-Ir sol drop dried on a carbon coated molybdenum micro grid was measured in a FEI Titan Themis 200 kV Cs-corrected TEM with 0.09 nm HRTEM and 0.16 nm STEM resolution equipped with 4 Thermofischer EDS detectors. Measured data were evaluated and elemental maps were created by using the Velox software.

UV–Vis spectra of the supported samples were recorded by an Agilent Cary 60 spectrometer with a DRA accessory in diffuse reflectance mode to compare the localized surface plasmon resonance (LSPR) of metallic nanoparticles.

The crystalline components of the catalysts were investigated by **X-ray powder diffraction (XRPD)** analyses by a Philips model PW 1710 based PW 1820 Bragg-Brentano parafocusing goniometer using Cu Kα radiation (λ = 0.15418 nm), graphite monochromator and proportional counter. The digitally recorded XRPD scans were evaluated for quantitative phase composition using a full profile fit method with corrections for preferred orientation and microabsorption.

Temperature programmed oxidation and reduction (TPO, TPR) of the catalyst samples were measured in a complex catalyst characterization apparatus (Autochem 2920, Micromeritics) equipped with a Pfeiffer quadrupole mass spectrometer. TPO of the as prepared samples up to 400 °C were carried out followed by 1 h isothermal period recording the m/e = 44 signal of CO_2 evolved due to oxidation of residues of PVA stabilizer. In a consecutive step, the TPR of the calcined samples were followed by a thermal conductivity detector (TCD), and the water, which was produced during the reduction process, was trapped before the detector. The temperature ramps and the gas flow rates of 10 % O_2/He and 10 % H_2/Ar used in these experiments were 10 °C/min and 50 mL/min, respectively.

The Ru-containing samples and the monometallic Au/Al_2O_3 were investigated also by **X-ray photoelectron spectroscopy (XPS)** using a KRATOS XSAM 800 XPS machine equipped with an atmospheric reaction chamber. Al Kα characteristic X-ray line, 40 eV pass energy and FAT mode were applied for recording the XPS lines of Au 4f, Ru 3d, O 1s, C 1s, Al 2p regions. Al $2p_{3/2}$ binding energy at 74.4 eV was used as reference for compensation of charging effect. The samples were measured in as prepared state, after in situ calcination (400 °C/20 % O_2 in N_2/1 h) and after a consecutive reduction (350 °C or 400 °C/H_2/30 min in case of Au/Al_2O_3 and AuRu/Al_2O_3, respectively) pretreatment.

CO adsorption followed by DRIFT spectroscopy (CO-DRIFTS) was applied to study the interaction of CO with the surface of the catalysts using a Nicolet is50 FTIR spectrometer equipped with an MCT detector, a Specac DRIFT accessory and a Specac environmental chamber with a ZnSe window. 64 scans were collected for all spectra with a resolution of 4 cm^{-1}, and presented as log(1/R) using a proper background spectrum, where R is the reflectance. In each experiment, approximately 60 mg of sample pretreated ex situ under synthetic air flow (100 mL/min) at 400 °C for 1 h ("calc" sample) was loaded into the environmental chamber. CO adsorption was observed on the ex situ pretreated sample (as received). The spectra were recorded at room temperature under 1% CO in He flow after 5 and 10 min exposure, then after five minutes flushing with argon. Following that, other consecutive in situ treatments were performed and this CO adsorption measurement repeated to test the changes on the surface after each treatment. The first one was carried out in Ar at 400 °C for 5 min followed by an in situ oxidation in synthetic air at 400 °C for 5 min, the cooling was performed in the treating gases. After that, the samples were reduced for 40 min in 5% H_2 in Ar at 350 °C in case of Au/Al_2O_3 and at 400 °C in the other cases and then cooled down under Ar flow. This was followed by a stronger reduction in 5% H_2 in Ar at 500 °C for 30 min with cooling under Ar flow. The last step was a re-oxidation in synthetic air at 400 °C for 10 min in case of Au/Al_2O_3 and AuRu/Al_2O_3 and for 30 min in case of the other samples. The gas flow in the infrared spectrometer was always 30 mL/min. For the CO adsorption spectra, the ones measured just before the CO admission were used as background. This presentation depicts only the spectral changes due to CO adsorption. The Ir containing samples were exceptions, in these cases the room temperature spectra of the samples after the 400 °C in situ treatment in Ar were applied as background for all the next CO adsorption measurements, since some CO was retained on the surface in the consecutive treatments. The CO gas spectrum was subtracted from the spectra recorded under 1% CO/He flow, and in this way the bands of CO adsorbed became more noticeable.

2.4. Catalytic test

The catalytic activity for benzyl alcohol oxidation was evaluated in a 50 mL three necked glass reactor equipped with a reflux condenser. The temperature and stirring of the reaction mixture was provided by an electronically controlled heated magnetic stirrer. The oxygen was bubbled into the reaction mixture with 150 ml/min. 0.3 ml (2.9 mmol) of benzyl alcohol and 29.7 mL of toluene, with 400 mg K_2CO_3 and also without K_2CO_3 were loaded into the reactor, then preheated to 80 °C under stirring (1350 rpm) and the oxygen flow was turned on. After 20 min the reaction was initiated by the addition of 15 – 30 mg catalyst to the reaction mixture. Samples of 0.5 mL were collected every 10 min for 50 min and a later sample was collected at about 2.5 h. The samples were filtered and 1 V/V% of dodecane (internal reference) was added in 1 to 1 ratio. The mixture was analysed with a CHROMPACK CP 9000 type gas chromatograph (GC) equipped with a FID detector using a CP-Sil-5-CB (50.0 m x0.32 mm x1.19 μm) capillary column. Two kinds of catalysts were tested: the one which were just calcined ("calc" samples) and other which received a calcination and then a reduction pretreatment ("red" samples). The initial reaction rate was determined from the slope of the first 3 points of the conversion curves if these were close to linear, and expressed as converted benzyl alcohol (mmol) per hour related to 1 g catalysts and also to 1 mmol of metal (Au + Ru or Ir). When the initial part of the conversion curves showed increasing slope (induction period), the reaction rate was calculated from the slope of the linear part after the induction period.

3. Results and discussion

3.1. Structure of the catalysts

Table 1 shows the measured metal loading and the average particle size of the samples. The gold loading determined by PGAA well met the nominal values in all catalysts, but the ruthenium and iridium loading was much less than the nominal one in case of the sol-derived samples. Therefore, the Au/Ru and the Au/Ir molar ratios were higher than the intended 1/1. We believe that the reduction of ruthenium and iridium by $NaBH_4$ was not complete, however, gold enhanced the efficiency of their reduction, similarly as in ref. [41]. The limited reduction of iridium precursor ions by $NaBH_4$ at room temperature and its accompanying hydrolysis was reported in the literature [42]. The Ir/Al_2O_3 was prepared by wet impregnation, because by the sol adsorption method only a very low metal content could be attained. The metal loading of the impregnated sample corresponded to the theoretical one.

Fig. 1 presents a typical **TEM** image of all the catalysts in calcined and reduced states. All the samples except Ru/Al_2O_3 showed even distribution of spherical particles containing Au/Ru/Ir with narrow size distribution. Among the gold containing samples the Au/Al_2O_3 had the lowest mean diameter (about 2 nm (Fig. 1a, b)), while in the AuRu/Al_2O_3 (Fig. 1c, d) and AuIr/Al_2O_3 (Fig. 1e, f) it was about 4 and 5 nm, respectively. There was no significant difference between the calcined and reduced states in these cases. On the calcined Ru/Al_2O_3 the

Table 1
Metal loading and average particle diameter of the catalysts determined by PGAA and TEM, respectively, and H_2 consumption measured in TPR.

Catalysts	Metal loading						Average particle diameter		H_2consumption in TPR of the calcined samples
	μmol/g_{cat}			wt%			nm		% [c]
	Au	Ru	Ir	Au	Ru	Ir	calc (400 °C/air/1h)	red (400 °C/H_2/0.5h)	
Au/Al_2O_3	91	–	–	1.80	–	–	1.9 ± 0.5	2.1 ± 0.7 [a]	
Ru/Al_2O_3	–	49	–	–	0.50	–	11.3 ± 3.7	– [b]	51
$AuRu/Al_2O_3$	47	35	–	0.93	0.35	–	3.8 ± 1.4	3.7 ± 1.1	78
Ir/Al_2O_3	–	–	187	–	–	3.6	0.6 ± 0.3	1.5 ± 0.8	92
$AuIr/Al_2O_3$	49	–	14.6	0.97	–	0.28	5.1 ± 1.5	5.0 ± 1.5	82

[a] Reduction was performed at 350 °C/H_2/0.5 h.
[b] The sample was very heterodisperse and anisometric.
[c] H_2 consumed as % of the theoretical consumption in the reduction of all the ruthenium/iridium from RuO_2/IrO_2 to metallic Ru/Ir.

ruthenium formed big (around 11.3 nm) spherical particles (Fig. 1g). The dispersion of the Ru-oxide particles changed after reduction, the size distribution widened, both larger anisometric particles and small ones were observed (Fig. 1h). In case of Ir/Al_2O_3 the wet-impregnation preparation method followed by calcination resulted in very small iridium oxide particles with mean diameter of 0.6 nm (Fig. 1i). Aggregation was observed during the reduction providing 1.5 nm mean diameter still smaller compared to all the other catalysts (Fig. 1j).

The NPs of the Au-Ru and Au-Ir sols were examined with **STEM-EDS**. With this technique the distribution of gold and ruthenium or iridium within a single particle could be determined due to the close to atomic-level resolution. The 18 particles of the **Au-Ru sol** measured were all bimetallic, and the mean molar Au composition was Au/(Au + Ru) = 53 ± 23 % very close to the bulk value (57 %). On the Au and Ru elemental maps of the particles (see Fig. 2 and Fig. S1) the gold appears in the centre and the ruthenium beside some in the centre rather in the outer part, shell of the metal particles. This suggests that the particles had Au(-Ru) core (the exact composition of the core could not be determined from the Au and Ru maps) with Ru shell type structure, but the ruthenium did not fully cover the gold. The co-reduction of Au and Ru did not result in well mixed alloy particles, ruthenium accumulated rather on the surface of the bimetallic particles possibly due to the lower reduction rate of $RuCl_3$ compared to $HAuCl_4$ as was observed also in sonochemical co-reduction of these precursors [41]. Similar structures evolved in different preparation procedures have been observed in many articles [20,43–45]. There are reports of interactions between gold and ruthenium in spite of that alloy formation was not detected [44,45], but formation of solid solution alloy with various Au/Ru ratio was confirmed in polyol reduction method [46].

In **Au-Ir sol** the 22 particles examined by STEM-EDS were all bimetallic, as well. The typical distribution of Au and Ir in these particles is presented on Fig. 3 and Fig. S2. Similar distribution of Au and Ir were found and reported to be mixed alloy particles in $AuIr/TiO_2$ produced by sequential deposition precipitation with urea followed by reduction at 500 °C in hydrogen [47]. In the Au-Ir sol particles could not be observed such a well visible core-shell type structure as in case of Au-Ru sol, however some small enrichment of Ir on the outer surface can be suspected on the Au and Ir maps. The mean Au molar composition of the particles was Au/(Au + Ir) = 61 ± 10 %, which is somewhat lower than the bulk value (77 %). This means that particles of higher Au content should have been too in the sol. In case of seven particles the composition of their inner part could also be calculated with acceptable error. In five of these the Au/Ir ratio was significantly higher, than in the whole particles (in two of these it was about the same), thus supporting the suspect of some enrichment of Ir on the surface.

The supported bimetallic samples were investigated by **XRPD** in as prepared and calcined states, while the monometallic Ru/Al_2O_3 and Ir/Al_2O_3 in calcined and reduced forms. The XRPD scans are shown in Fig. S3. The reflections of the crystalline phases of the active catalyst components (gold, ruthenium, iridium) were superimposed with those of the support (containing γ- and δ-alumina). So the position and line broadening of the peaks could be determined only by a full profile fitting procedure with relatively low precision. The XRPD scan of the as prepared **$AuRu/Al_2O_3$** could be well fitted with the peaks of the support and 4 nm fcc Au and 4 nm hexagonal Ru crystallites. Similar size of metallic particles was measured by TEM as well, but the Ru and Au could not be distinguished. In calcined $AuRu/Al_2O_3$ beside metallic gold of 5 nm crystallite size only RuO_2 (and no metallic ruthenium) with quite narrow reflections appeared (large crystallites, 90 nm), but the co-presence of much smaller crystallites cannot be ruled out. In the TEM images such large particles were not observed, likely those were in very low concentration. Both as prepared and calcined **$AuIr/Al_2O_3$** presented Au reflections with line broadening indicating about 5 nm size (again in quite good correspondence with sizes measured by TEM), but no reflections of metallic iridium, neither Ir-oxide. The low concentration Ir (0.3 wt%) may have been highly dispersed or alloyed with gold. In case of both Au-Ru and Au-Ir bimetallic samples no significant shift of the Au reflections (neither of the metallic Ru ones in the as prepared $AuRu/Al_2O_3$) could be discerned referring to notable extent alloying. In the XRPD spectrum of the calcined monometallic **Ru/Al_2O_3** lines of RuO_2 (with no noticeable metal) were well visible, while in its reduced state metallic Ru (with no perceptible oxide) reflections indicating about 30 nm size in both cases, which is somewhat larger than that observed by TEM. In the calcined **Ir/Al_2O_3** Ir containing crystalline phases did not appear on the contrary of high loading (3.6 wt% Ir), in agreement with the small size (0.6 nm) determined by TEM. In the reduced form metallic Ir phase could be fitted with 3 nm size, but with low concentration, that can be attributed to the larger size fraction of Ir particles of 1.5 ± 0.8 nm mean diameter.

UV–Vis spectra of the supported samples in as prepared, calcined and reduced states are collected on Fig. 4. For **Au/Al_2O_3** the characteristic localized surface plasmon resonance (SPR) band was at 518 nm (Fig. 4a) in the as prepared and reduced state. In calcined form only a small red shift compared to these was observed (from 518 to 524 nm) indicating the presence of metallic Au NPs in all states. The different pretreatments significantly changed the spectra of the monometallic **Ru/Al_2O_3** (Fig. 4b) and **Ir/Al_2O_3** (Fig. 4c). In the calcined state both of them present two wide bands, Ru/Al_2O_3 at 400 and 780 nm, Ir/Al_2O_3 at 368 and 646 nm. Similar bands were observed by others at 775 nm for hydrous RuO_2 [48] and at 574 nm for IrO_2 [42,49] NPs in aqueous solutions. On the other hand a band at 430 nm measured on Ru-oxide/hydroxide deposition-precipitated on TiO_2 was assigned to d-d transition band, what disappeared on reduction by H_2 [20], and a band observed at 315 nm in case of hydrolysed Ir^{3+} was attributed to $Ir(OH)_6^{2-}$ [42]. In reduced state no characteristic band was found in the spectrum of Ir/Al_2O_3, but in case of Ru/Al_2O_3 a wide band appeared with weak maxima around 400 and 570 nm that may indicate some hydroxide/oxide content beside metallic Ru NPs, which latter according to literature does not show any obvious band in the visible region [20,41,46] as neither metallic Ir NPs [50]. The as prepared

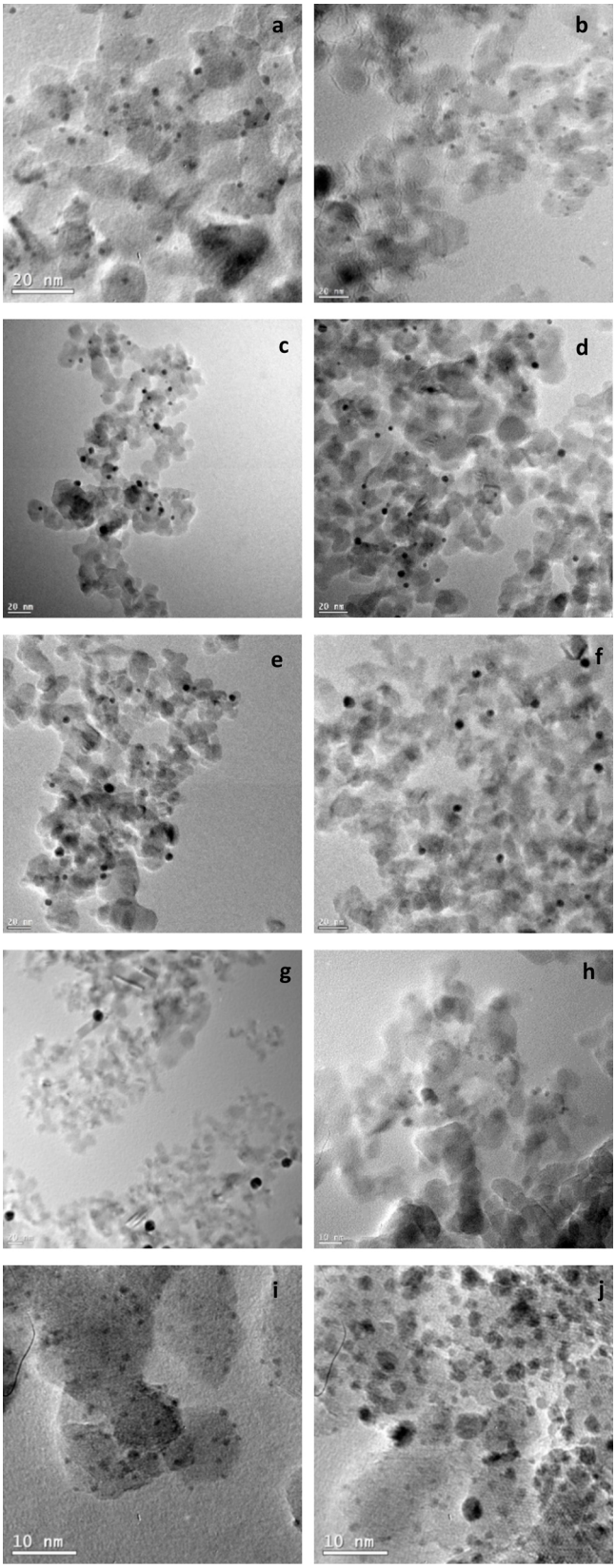

Fig. 1. Representative TEM images of the catalysts in calcined (images on the left) and reduced states (images on the right). Au/Al_2O_3 (a, b), $AuRu/Al_2O_3$ (c, d), $AuIr/Al_2O_3$ (e, f), Ru/Al_2O_3 (g, h), Ir/Al_2O_3 (i, j).

$AuRu/Al_2O_3$ (Fig. 4d) does not show the band typical of Au NPs, it is quite similar to the as prepared Ru/Al_2O_3 superimposed with a wide very weak band around 600 nm. This is likely due to the Au core/Ru shell type structure suggested by elemental maps of single particles. A damping and small red shift of the SPR band of Au NPs due to the formation of Ru overlayer was experienced also by others [41]. In case of calcined state, however, a clear band appears at 524 nm just as for the corresponding Au/Al_2O_3 sample, accompanied by features around 400 and 800 nm as for calcined Ru/Al_2O_3. In reduced state the spectrum of the Au-Ru bimetallic sample seems to be the superposition of the spectra of the reduced monometallic ones with a tiny red shift of Au. These imply decreased interaction of metallic Au and Ru-oxide during calcination, and the subsistence of increased separation of Au and Ru under reduction producing metallic Ru. Concerning **$AuIr/Al_2O_3$** (Fig. 4e) the situation is somewhat different. The characteristic band of Au NPs is well visible in all states slightly red shifted compared to Au/Al_2O_3, more in as prepared state. Thus we suggest that there is some interaction between Au and Ir in all states. Additional band is visible at 368 nm in calcined state resembling the spectrum of the calcined Ir/Al_2O_3 of more than ten times higher Ir loading, but its band around 646 nm is missing in the bimetallic spectrum.

The as prepared supported samples contained residues of stabilizing agent that could not be completely removed by the washing applied, as shown by the CO_2 evolution during the **TPO** of the as prepared samples (Fig. S4). In all cases the maxima of CO_2 evolution bands assigned to the combustion of organics in the vicinity of the metal NPs are well below 400 °C. So we believe that the applied calcination treatment provided clean active surface for a more reliable comparison of the different catalysts. Since the calcination may oxidize also Ru and Ir, a following reduction was carried out as well. The samples were studied both in calcined and reduced states.

The TPR curves of the calcined samples are depicted in Fig. 5 and the H_2 consumptions are given in Table 1 in % of the theoretical consumption calculated for reduction of all the ruthenium or iridium from RuO_2 or IrO_2 to metallic Ru or Ir.

There was significant H_2 uptake in all cases except the monometallic gold. Iridium in calcined Ir/Al_2O_3 presumably was fully oxidized to IrO_2, the most stable Ir-oxide, what could be close to fully reduced up to 400 °C, since the H_2 consumption almost reached the theoretical value. In the bimetallic $AuIr/Al_2O_3$ sample the somewhat lower H_2 consumption (82 %) may indicate rather the presence of some metallic Ir in calcined state, than remaining oxide after reduction, since even the highly dispersed IrO_2 in calcined Ir/Al_2O_3 could be reduced. The only, but wide H_2 consumption peak in case of the monometallic sample was centred at lower temperature (153 °C), than the also wide main peak of the bimetallic $AuIr/Al_2O_3$ catalyst at 258 °C, which was accompanied by a small peak at 60 °C. Possibly a small part of IrO_2 in intimate interaction with gold was reduced at this low temperature, while the more separated IrO_2 presented the reduction at 258 °C. In the literature two-three various temperature reduction peaks between 70 and 450 °C were reported in TPR of calcined Ir on various supports (SiO_2 [51], Al_2O_3 [52,53], TiO_2 [34]). The lower temperature peaks were assigned generally to larger, the higher temperature ones to smaller particles. Our calcined Ir/Al_2O_3 of extremely high IrO_2 dispersion could be reduced at lower temperature compared to other published Ir/Al_2O_3 catalysts that might be due to the relatively high loading of Ir and closeness of oxide particles on the support surface. The H_2 dissociated on the firstly reduced Ir sites could spill over easily to neighbouring IrO_2 and reduce them. In TPR of a calcined (at 500 °C) $AuIr/TiO_2$ Ir was reduced in higher temperature steps, than in the corresponding monometallic Ir catalyst (at 270 and 510 °C versus 145, 180, 300 °C) [35], similarly as in our case. Our Ru/Al_2O_3 and $AuRu/Al_2O_3$ samples consumed only 51 % and 78 %, respectively, of the theoretical amount calculated for the RuO_2 reduction to metallic Ru for the total amount of Ru. It means that Ru was not fully oxidized in calcination or/and not fully reduced in reduction up to 400 °C. Both Ru-containing catalysts

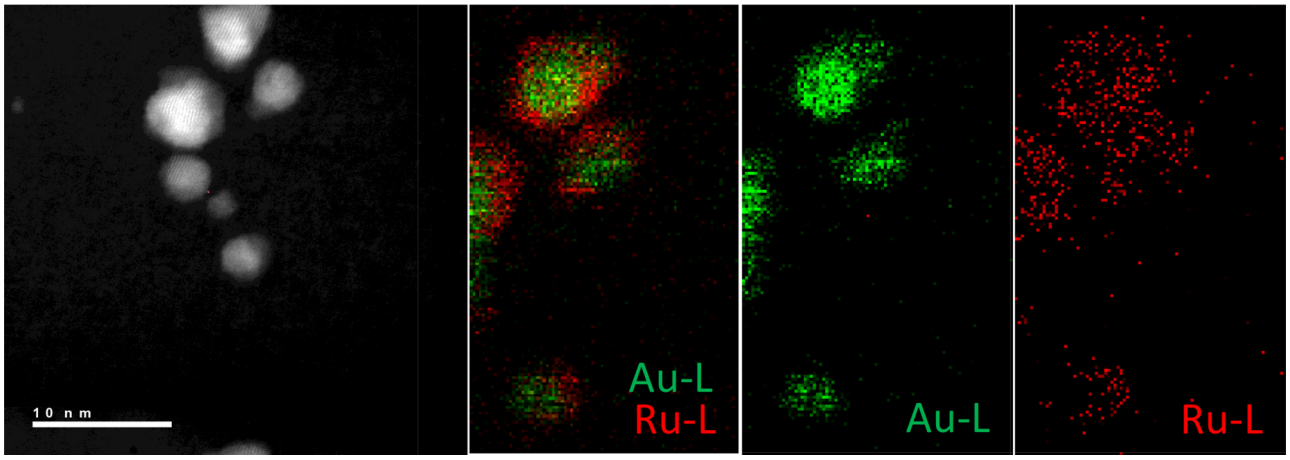

Fig. 2. HAADF image (a) with STEM-EDS Au(L) (green) and Ru(L) (red) maps (b-d) of the Au-Ru sol. (For interpretation of the references to colour in this figure legend, the reader is referred to the web version of this article).

presented two reduction bands. These peaks likely indicate RuO_2 phases in different size and interaction with the support or with gold in the bimetallic sample. One of these at about 75 °C in both cases is assigned to the larger particles in no interaction with Au. The second peak appeared at 107 °C for $AuRu/Al_2O_3$ and a very weak one at 318 °C for Ru/Al_2O_3 likely belonging to the more dispersed RuO_2, in the former case contacting with Au that favours its reduction [18].

The oxidation state of Ru and Au was studied by **XPS** as well in the $AuRu/Al_2O_3$ catalyst in comparison with the monometallic ones. On Fig. 6 the Ru 3d overlapping with C 1s binding energy region and the spectra of Au 4f are collected for the bimetallic and the monometallic samples in as prepared, calcined and reduced states. In Figs. S5 and S6 the deconvolution of all the XPS spectra can be seen. The binding energy (BE) values of the different components of the spectra are reported in Table 2.

Regarding ruthenium, two states could be distinguished in the as prepared and calcined **$AuRu/Al_2O_3$**. One of them with BE at 280.3 (as prep.) and 280.5 eV (calc.), which is very similar the only one at 280.7 eV in the reduced state, and thus it is assigned to metallic Ru. The other peak at 282.9 and 281.8 eV of the as prepared and calcined forms may belong to Ru-hydroxide formed beside metallic Ru in the reduction by $NaBH_4$ below room temperature (similarly as reported for iridium reduction by $NaBH_4$ [42]) and RuO_2, respectively [54]. It is worth to note that in the calcined state about 30 % of surface Ru remained in metallic state well agreeing with TPR (H_2 consumption was 78 % of the theoretical one), since all Ru-oxide could be reduced, only metallic Ru was detected after the in situ reduction. The surface concentration of Ru was much higher, than that of gold on the contrary of the Ru/Au = 0.74 bulk atomic ratio. It increased in the consecutive treatments, though the appearance of large RuO_2 crystallites after calcination was revealed by XRD. So Ru enriched on the surface and a fraction of that was possibly in high dispersion at least partly on Au particles.

In the monometallic **Ru/Al_2O_3** Ru 3d states of lower BEs than in the bimetallic sample were observed. In all states of this sample two Ru $3d_{5/2}$ peaks could be distinguished, one around 279.2–279.7 eV (metallic Ru) and the other at 281.3–281.5 eV (RuO_2) in different intensity ratio, the most metallic Ru was in the reduced sample. The higher BE of metallic Ru in the bimetallic sample might be due to the interaction with gold. On the contrary, in case of solid-solution alloyed Au-Ru particles opposite shift (to lower BE) of Ru peaks were observed accompanied by the increase of Au 4f binding energy and assigned to electron transfer from gold to ruthenium [46]. The not complete oxidation and reduction of Ru in the calcined and reduced state, respectively, suggested by XPS corresponds with the TPR results. In the bimetallic sample gold favoured the reduction of RuO_2. The surface Ru concentration of the monometallic Ru sample was similar to that in the as prepared bimetallic sample, but in the calcined and reduced forms it dropped by 50–60 % (in the bimetallic increased), so it became much lower, than that in $AuRu/Al_2O_3$. It was lower also than the surface atomic concentration of Au in Au/Al_2O_3 in agreement with the markedly larger particle size and lower molar concentration of Ru measured in Ru/Al_2O_3.

The main component of the Au 4f bands was at the same BE (83.1–83.4 eV) in all states of both **$AuRu/Al_2O_3$** and monometallic **Au/Al_2O_3** and assigned to metallic Au. Beside that at higher BE another, a partially positively charged Au state was observed on the as prepared

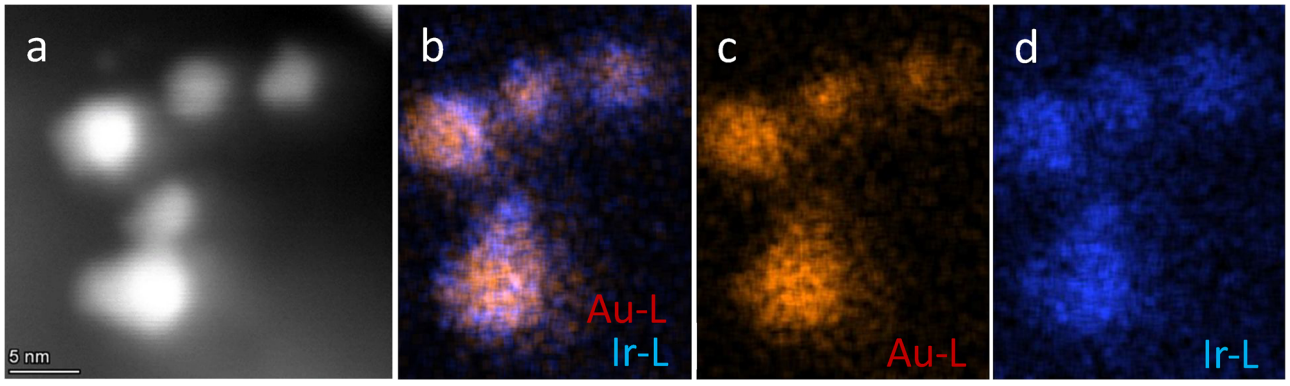

Fig. 3. HAADF-STEM image (recorded before the STEM-EDS) (a) with STEM-EDS Au(L) (orange) and Ir(L) (blue) maps (b-d) of the Au-Ir sol. (For interpretation of the references to colour in this figure legend, the reader is referred to the web version of this article).

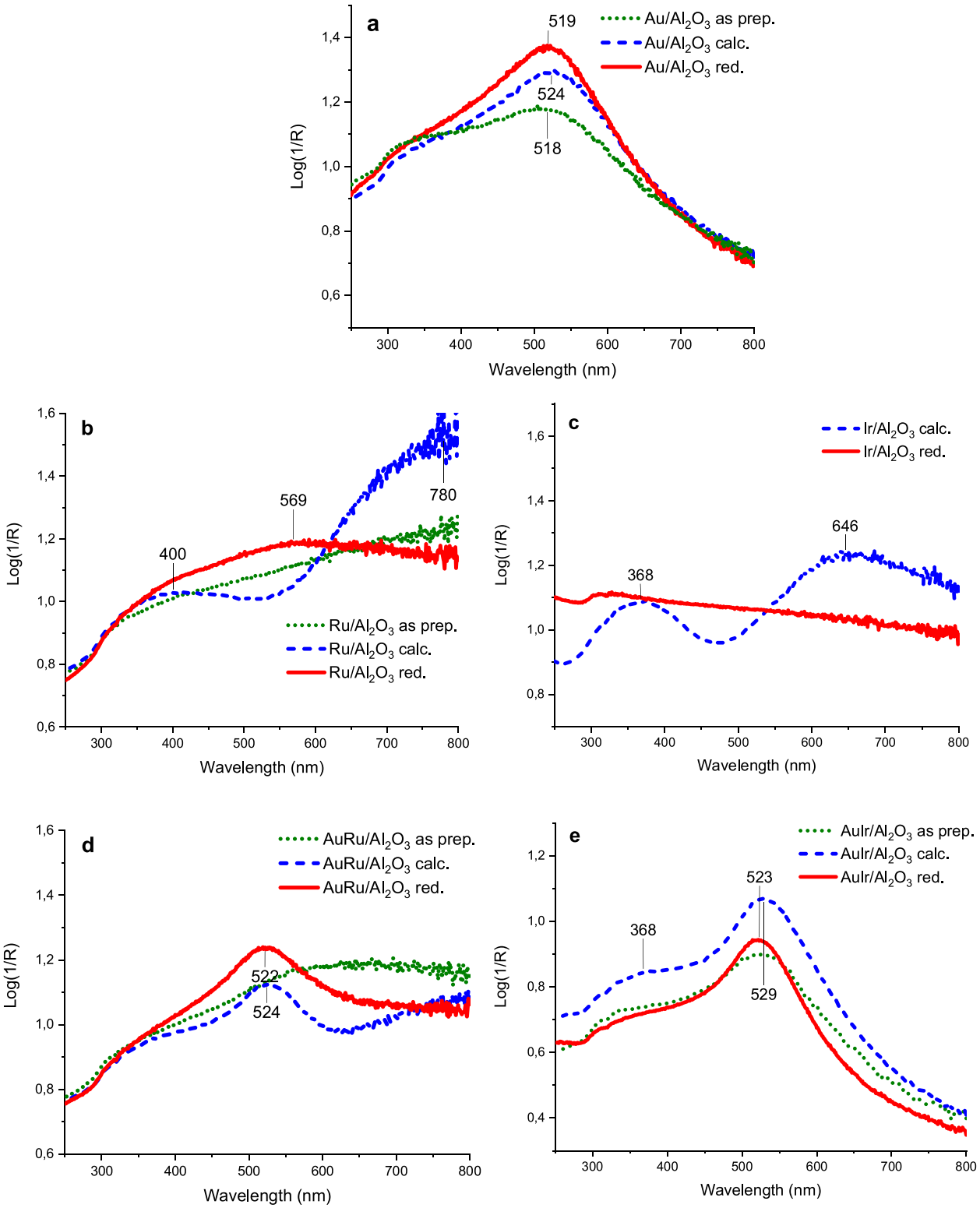

Fig. 4. UV–Vis spectra of Au/Al_2O_3 (a), Ru/Al_2O_3 (b) Ir/Al_2O_3 (c), $AuRu/Al_2O_3$ (d) and $AuIr/Al_2O_3$ (e) samples, in as prepared (green curves), calcined (blue curves) and reduced (red curves) states. (For interpretation of the references to colour in this figure legend, the reader is referred to the web version of this article).

and calcined Au-Ru (at 84.5 eV in lower ratio in the latter state) and on the as prepared monometallic Au sample (at 85.6 eV). This could be assigned to Au interacting with PVA residues in as prepared states and in the bimetallic catalyst with Ru-hydroxide or Ru-oxide in the as prepared and calcined states. The similar surface Au concentration in calcined and reduced state (the Au particle size was also almost the same) was lower a bit than in the as prepared one.

3.2. Topmost surface characterization by CO adsorption followed by DRIFT spectroscopy

The surface composition of the metal particles after different pre-treatments was studied by CO adsorption followed by DRIFTS measurements. This technique analyses the topmost surface of the sample, where the catalytic reaction takes place. The IR spectra of the adsorbed

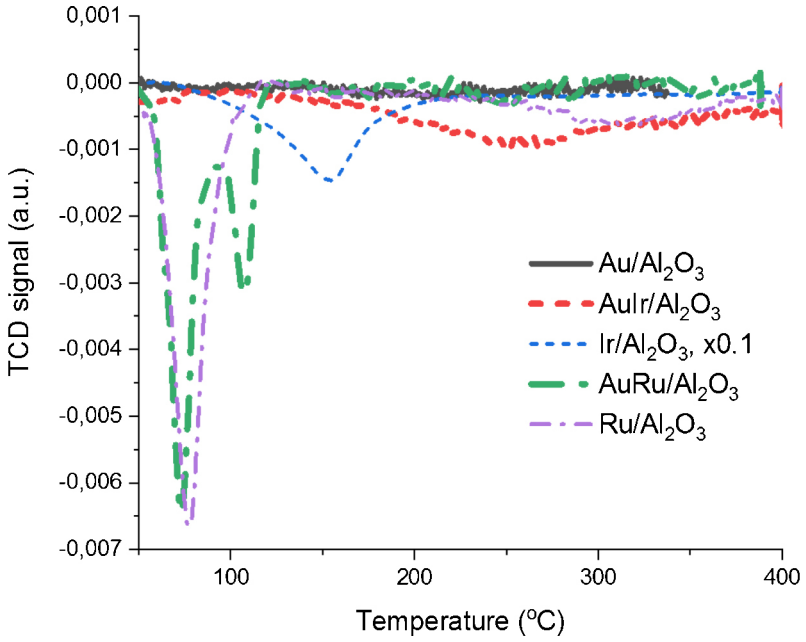

Fig. 5. TPR of the calcined samples.

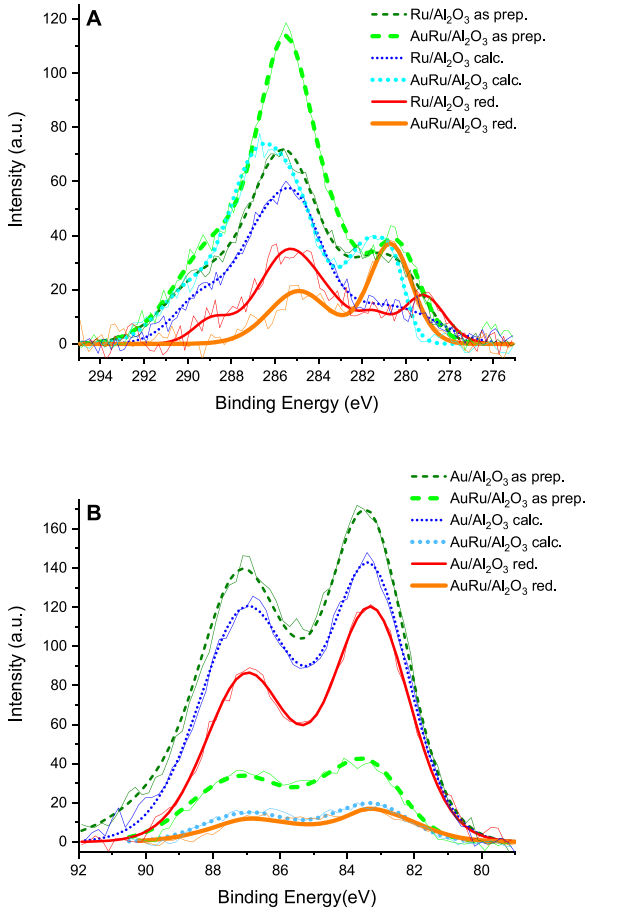

Fig. 6. Ru 3d with C 1s (A) and Au 4f XPS (B) spectra (background was subtracted) of $AuRu/Al_2O_3$, Au/Al_2O_3 and Ru/Al_2O_3 in as prepared, in situ calcined and in situ reduced states (The measured spectra are the light lines, the envelopes of the fitted peaks are the heavy dashed, dotted or straight lines).

Table 2
The Ru $3d_{5/2}$ and Au $4f_{7/2}$ binding energy (BE) values and Ru and Au surface concentrations of $AuRu/Al_2O_3$, Ru/Al_2O_3 and Au/Al_2O_3 samples after different in situ treatments.

Ru $3d_{5/2}$ BE	Ru concentration		Au $4f_{7/2}$ BE	Au concentration		Ru/Au
eV	at. %		eV	at. %		at. ratio
$AuRu/Al_2O_3$_as prep.						
282.9	0.049	0.118	84.6	0.016	0.075	1.6
280.3	0.069		83.2	0.059		
ASAuRu2_calc.						
281.8	0.090	0.130	84.5	0.006	0.057	2.3
280.5	0.040		83.2	0.051		
$AuRu/Al_2O_3$_red.						
280.7	0.129	0.129	83.1	0.050	0.050	2.9
Ru/Al_2O_3_as prep.			**Au/Al_2O_3_as prep.**			
281.3	0.100	0.129	85.6	0.03	0.19	
279.7	0.029		83.4	0.16		
Ru/Al_2O_3_calc.			**Au/Al_2O_3_calc.**			
281.3	0.031	0.058	83.1	0.15	0.15	
279.4	0.027					
Ru/Al_2O_3_red.			**Au/Al_2O_3_red.**			
281.5	0.011	0.051	83.2	0.14	0.14	
279.2	0.040					

CO are shown in Fig. 7.

On **Au/Al_2O_3** the adsorbed CO band appeared at 2106 cm^{-1} after ex situ calcination, heat-treatment in Ar and reductions (Fig. 7/A a,b,d and e curves). This band was assigned to the CO adsorbed on low coordinated surface Au^0 atoms [55,56]. Among the catalysts only the monometallic gold is capable of the adsorption of CO after ex situ calcination, which calcined sample was contacted with the atmosphere. So the surface of monometallic gold nanoparticles likely adsorbed fewer substances (like water) from the environment than the other catalysts or it was easier to remove the contamination from its surface by flushing with Ar at room temperature. Therefore, the CO was able to adsorb on the rest of gold surface or was able to supplant the contamination. Following a short in-situ 400 °C pretreatment in Ar the Au surface became even more accessible and the CO band at the same position increased somewhat.

After in situ calcination (Fig. 7/A c curve) and also recalcination (Fig. 7/A f curve) the CO band shifted to a higher wavenumber and the

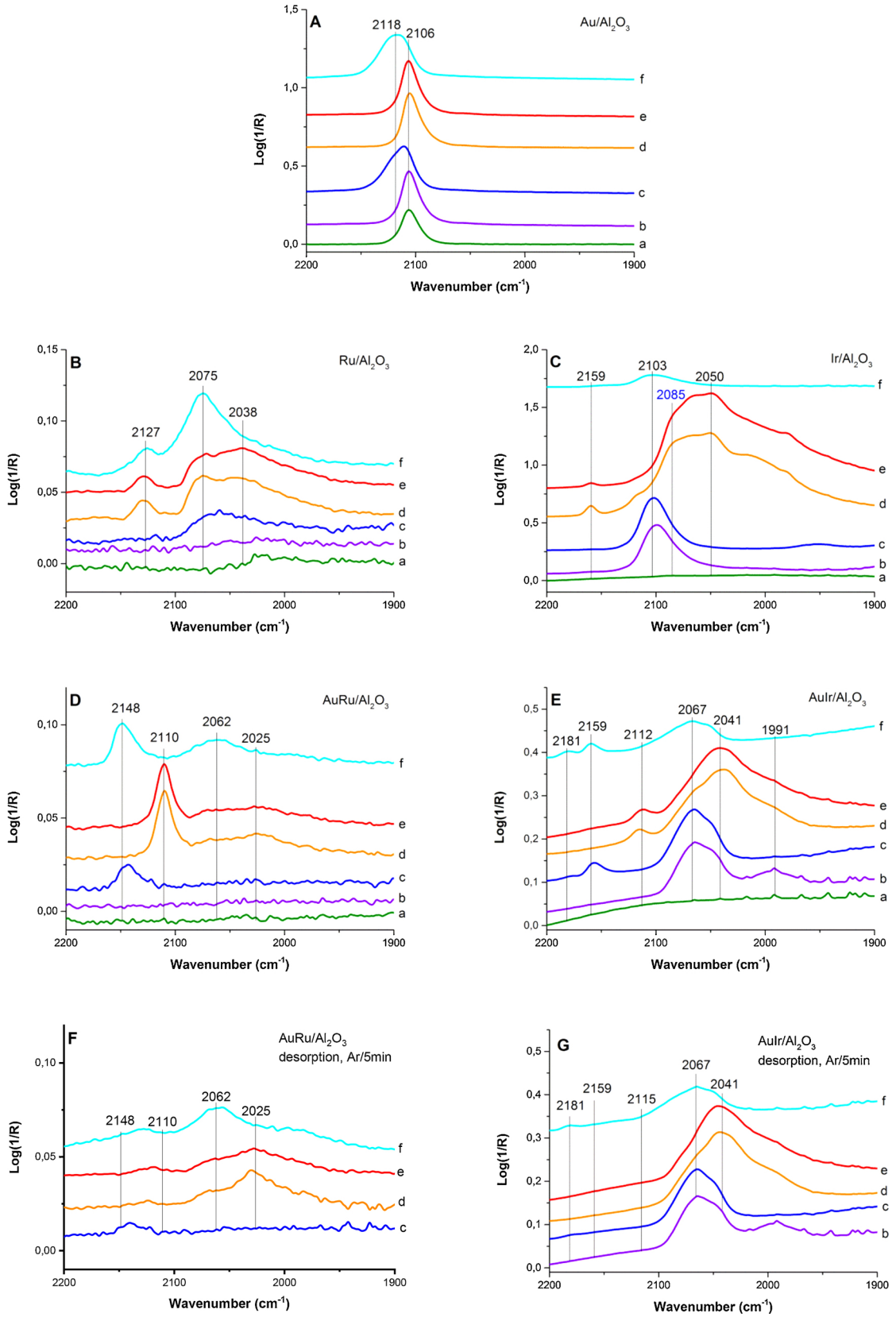

Fig. 7. DRIFT spectra of CO adsorbed at RT in presence of 1% CO/He after different consecutive pretreatments on Au/Al_2O_3 (A), Ru/Al_2O_3 (B), Ir/Al_2O_3 (C), $AuRu/Al_2O_3$ (D) and $AuIr/Al_2O_3$ (E) and adsorbed CO retained after 5 min purging in Ar on $AuRu/Al_2O_3$ (F) and $AuIr/Al_2O_3$ (G) Pretreatments: a) (green) ex situ calcination (Air/400 °C/1 h); b) (purple) Ar/400 °C/5 min; c) (blue) in situ calcination (Air/400 °C/5 min); d) (orange) reduction (5% H_2 in Ar/350 °C or 400 °C/40 min) cooled in Ar; e) (red) reduction (5% H_2 in Ar/500 °C/30 min) cooled in Ar; f) (light blue) recalcination (Air/400 °C/10 or 30 min). (For interpretation of the references to colour in this figure legend, the reader is referred to the web version of this article).

shape of the peak became wider. This shift was decreasing back to 2106 cm^{-1} with time in presence of CO. The shift refers to $Au^{\delta+}$ that the CO could reduce. It correlates with that reported by Mihaylov and coworkers, namely the bands in the 2130–2090 cm^{-1} region have been assigned to Au^0–CO species, and the bands in the 2155 − 2130 cm^{-1} region have been attributed to CO on positively polarized gold [56]. The shift was larger in case of reoxidation (2118 cm^{-1} (Fig. 7/A f curve)) than in the first in situ calcination (2111 cm^{-1} (Fig. 7/A c curve)) possibly due to the longer calcination. But there was no shift on the ex-situ calcined state (Fig. 7/A a curve). This and the reductive effect of CO at room temperature well showed that the gold nanoparticles lose easily their partial positive charge formed due to oxidation at elevated temperature. Reduction at 350 and 500 °C restored roughly the same surface as after the initial 400 °C/Ar pretreatment presenting similar CO adsorption spectra.

On the samples which contained ruthenium or iridium the spectra of CO adsorption were complex. On the **Ru/Al_2O_3** (Fig. 7/B) was practically no adsorption after ex situ calcination and heat-treatment in Ar showing hardly any visible band (Fig. 7/B a and b curves). After a short in situ calcination a clear but still weak bands appeared around 2062 cm^{-1}. We think that the most of the ruthenium surface was still covered by some organic residues and water after ex-situ calcination, because the pretreatment at 400 °C/5 min desorbing normally the physisorbed volatile contaminations was not enough to completely clean the surface. But an additional short calcination liberated some more ruthenium sites. After reductions (Fig. 7/B d and e curves) new bands appeared at 2127, 2075, 2038 cm^{-1}. According to Hadjiivanov and co-workers the band of Ru^0-CO appears between 2050 and 2000 cm^{-1} depending on the coverage, the band of Ru^{n+}-CO at 2080 cm^{-1} and the Ru^{n+}-$(CO)_x$ x = 2,3 has two bands at 2136 cm^{-1} and 2080 cm^{-1} [57]. Our results well correlated with these. In our sample it was well seen that the reduction was not complete, because much Ru^{n+} was left after both reduction treatments after those the spectra of CO adsorbed were very similar. However, there were clearly visible differences between the spectra after in-situ calcination and recalcination following the reduction treatments. (Fig. 7/B c versus f curve). In the spectrum recorded after in-situ calcination the peak at 2062 cm^{-1} assigned to Ru^{n+}-CO of low coverage increased and shifted in the recalcined state to 2075 cm^{-1} due to the enhanced coverage and so dipol-dipol coupling and accompanied by formation of 2127 cm^{-1} as an indication of Ru^{n+}-$(CO)_x$, whose other, asymmetric stretching component at about 2080 cm^{-1} overlapped with the CO band of Ru^{n+}-CO. The presence of a weak component at 2038 cm^{-1} attributed to linearly adsorbed CO on metallic Ru cannot be ruled out. In the recalcined state the accessibility of Ru significantly increased, however the intensity of the ruthenium-adsorbed CO was still very small in all states examined, that can be partly due to the lower Ru loading and larger particle size (as shown by TEM and XRD) and lower surface concentration of Ru observed by XPS, than those of Au in monometallic Au/Al_2O_3.

In case of $AuRu/Al_2O_3$ (Fig. 7/D) and also $AuIr/Al_2O_3$ (Fig. 7/E) it was easy to distinguish the band of CO adsorbed on gold from those on ruthenium and iridium, because the gold adsorbs CO weakly, while the ruthenium and iridium adsorb it strongly. Therefore, after the samples were purged under Ar flow, only the Ru-CO and Ir-CO remained on the surface (Fig. 7/F and G). On the **$AuRu/Al_2O_3$** there was no absorption of CO after ex-situ calcination and in-situ heat treatment in Ar (Fig. 7/D a and b curves) as was observed also on Ru/Al_2O_3. After in-situ calcination only a peak of Au-CO was detected at 2143 cm^{-1} with very low intensity compared to Au/Al_2O_3. It correlates well with those in the 2200–2150 cm^{-1} region assigned to Au^+–CO species according to Mihaylov and coworkers [56]. This shows the interaction between the Au and Ru, since Ru increased the blue shift of the band of CO adsorbed on metallic Au (2106 cm^{-1}) in larger extent, than in case of calcined Au/Al_2O_3 (2118 cm^{-1}) showing larger and more stable positive charge of Au, higher concentration of Au^+ on Au NPs. On the other hand, no Ru-CO was detected. Fig. 7/D d and e curves show that after reduction weak overlapping bands of CO adsorbed on Ru appeared at 2062 cm^{-1} for Ru^{n+}-CO and at 2025 cm^{-1} for Ru^0-CO red shifted by 13 cm^{-1} compared to Ru/Al_2O_3. The proportion of Ru^0-CO was slightly higher compared to Ru^{n+}-CO, than in the monometallic sample suggesting higher reducibility agreeing with TPR and XPS results. The band of Au-CO shifted back to lower wavenumber (2110 cm^{-1}) indicating metallic gold, just slightly blue shifted (that might be due to Au interaction with Ru or lower CO coverage) compared to that on Au/Al_2O_3 (2106 cm^{-1}). After reoxidation (Fig. 7/D f curve) Au^+-CO appeared again as after the first in situ calcination, furthermore also a wide band at 2062 cm^{-1} was seen unlike after the first calcination, belonging to ruthenium, red shifted with respect to that measured on Ru/Al_2O_3 likely because of more separated Ru^{n+}-CO on likely more dispersed Ru over Au. More ruthenium sites became accessible on the surface due to the H_2-treatments as was observed on Ru/Al_2O_3 too. However, the amount of CO adsorbed on Ru in $AuRu/Al_2O_3$ was still very low on the contrary of higher surface atomic concentration of Ru, than on Ru/Al_2O_3 and also higher than that of Au in the bimetallic sample as measured by XPS. We suppose that the Ru surface was covered by some contamination, rather by some strongly attached organic ones or water and not by gold according to the largely reduced CO adsorption on gold compared to Au/Al_2O_3 and other results (STEM-EDS, XPS). The intensities of the Au-CO on the $AuRu/Al_2O_3$ were smaller than on Au/Al_2O_3 approximately by an order of magnitude, in much higher extent than we expected based on the gold loading and particle size, so the gold surface must have been largely covered by ruthenium.

The Fig. 7/C shows the spectra of the adsorbed CO on **Ir/Al_2O_3**. In spite of the fact that the CO bounded to the iridium very strongly (even the pretreatment at 500 °C/30 min was not able to desorb all the CO), there was no CO adsorption in case of ex-situ oxidation (Fig. 7/C a curve), because Ir must have been fully oxidized and its surface might have been blocked by adsorbates. The CO adsorption IR spectra after the heat-treatment in Ar (Fig. 7/C b curve) and the in situ calcination (Fig. 7/C c curve) were very similar, a large band appeared at 2103 cm^{-1} in both cases. It is tentatively assigned to coordinatively unsaturated Ir^{3+} on the Ir-oxide surface, since a CO adsorption band at 2100 cm^{-1} was observed by Gelin and co-workers investigating an Ir/NaFAU sample prepared using an Ir^{3+} precursor [58], and it was attributed to Ir^{3+}-CO species. Since no other CO band was found we think that all the iridium had already been in oxidized state after the ex-situ oxidation. Reducing the Ir/Al_2O_3 a wide, complex, intense band between 2100 − 1950 cm^{-1} evolved on CO admission (Fig. 7/C d and e curves). In these complex bands maxima or shoulders are visible at 2085, 2065, 2050, 2015, 1981 cm^{-1} with slightly different relative intensities. These bands indicate the co-presence of different Ir sites and type of CO adsorptions as linear carbonyls and dicarbonyls. In the literature various frequency IR bands of linear CO adsorption were reported on different size particles. Bands at 2075 − 2065 and 2050 − 2020 cm^{-1} were attributed to the linear CO adsorbed on larger particles and highly dispersed clusters of metallic Ir, respectively [59]. These bands red shifted with decreasing CO coverage. CO band pairs observed at 2070 and 1995 cm^{-1} were rendered to dicarbonyls on edge atoms of Ir rafts on alumina, others reported the formation of $Ir^+(CO)_2$ with CO band pairs at 2104 − 2088, 2037 − 2002 cm^{-1} on alumina and zeolite supported Ir [59,58,60]. The large proportion of dicarbonyl bands on our Ir/Al_2O_3 is in accordance with the high dispersion of Ir. Beside the complex band, a small single one appeared with a maximum at 2159 cm^{-1} (a similar band was related to Ir^{2+}-CO [60]) and a small shoulder at 2112 cm^{-1} after reduction at 400 °C, which decreased/disappeared after the sample had been reduced at 500 °C. After reoxidation (Fig. 7/C f curve) the peak at 2103 cm^{-1} had much lower intensity than after the first in-situ calcination (Fig. 7/C c curve) due to sintering of Ir, and again no sign of Ir^0-CO was discerned. The TEM measurements showed significant increase of iridium particle size after reduction at 400 °C (the mean particle diameter changed from 0.6 to

1.5 nm), so the dispersion of iridium particles greatly decreased.

On the **AuIr/Al_2O_3** (Fig. 7/E) no CO adsorption was observed in the ex situ calcined state, but after heating in Ar the band appearing at 2065 cm^{-1} with a shoulder at about 2050 cm^{-1} and the small band at 1991 cm^{-1} all stable under purging with Ar belonged to Ir. The former two were rather characteristic of linearly adsorbed CO on metallic Ir of different sites and the band at 1991 cm^{-1} may refer to a bridged carbonyl or with a component at around 2070 cm^{-1} to a dicarbonyl on metallic Ir. No sign of oxidized Ir was observed on the contrary to Ir/Al_2O_3, where only oxidized Ir^{n+} was depicted by adsorbed CO. Since TPR and also UV–Vis suggested the presence of the Ir-oxide in calcined state in AuIr/Al_2O_3 likely its surface was highly coordinated by oxygen or by hydroxyl and was not accessible for CO. In this state (Fig. 7/E b spectrum) no CO adsorbed on gold was detected, but after the short in situ calcination beside the same bands of Ir-CO another small one developed at 2157 cm^{-1} that quickly disappeared under purging with Ar and was assigned to CO adsorbed on Au^{+}. Similar, but lower intensity spectrum was observed after recalcination (see c and f spectra on Fig. 7/E and G). It was blue shifted related to the corresponding band measured on Au/Al_2O_3 (2118 cm^{-1}) and on AuRu/Al_2O_3 (2143 cm^{-1}) too, demonstrating an interaction between Au and Ir. After reductions the bands of CO adsorbed on iridium shifted to lower wavenumbers compared to the monometallic Ir/Al_2O_3. The complex band became sharper and more symmetric with a maximum at 2040 and shoulders at about 2067 and 1990 cm^{-1} indicating less types of CO species (Fig. 7/E d and e curves). No higher frequency bands belonging to Ir^{n+} adsorbed CO was discerned in any of reduced states, but metallic Au adsorbed CO presented a weak band at 2112 cm^{-1} blue shifted related to the Au/Al_2O_3 (2106 cm^{-1}) as in the case of AuRu/Al_2O_3 (2110 cm^{-1}) was observed. The gold showed very similar behaviour as in AuRu/Al_2O_3, the band intensities of the Au-CO were also much smaller, than in Au/Al_2O_3, thus we suppose high extent coverage of gold by the second metal iridium. To the better understanding we summarized the position of main CO bands and the assigned states of Au, Ru and Ir in the Table S1.

3.3. Catalytic properties

All catalysts were tested in benzyl alcohol oxidation both after calcination and subsequent reduction, with and without K_2CO_3 added. The conversion curves are collected in Fig. 8 a and b, the initial reaction rates calculated are summarized in Table 3. The benzaldehyde selectivity as a function of the benzyl alcohol conversion above around 20 % is presented on Fig. 8 c. It was always high, but decreasing with the increasing conversion, the lowest measured was 82 % at 85 % conversion on the calcined monometallic gold catalyst. The reduced Au/Al_2O_3 and AuIr/Al_2O_3 showed similar selectivity with AuRu/Al_2O_3 in both calcined and reduced states, while the calcined Au/Al_2O_3 and AuIr/Al_2O_3 were only slightly less selective at similar conversions.

The **Au/Al_2O_3** had a high initial activity in every case, but without K_2CO_3 the reaction almost stopped at about 15 % conversion (Fig. 8a), because the benzoic acid bounds very strongly to the gold surface, but the K_2CO_3 can prevent this [13,61]. With K_2CO_3 the deactivation was eliminated indeed and the reaction could reach a high conversion (almost 90 %) in about 150 min (Fig. 8b). It is interesting to note that in case of Au/Al_2O_3 the reduced catalysts were a little less active than the calcined ones. Since the DRIFTS measurement showed that the gold nanoparticles easily get and lose the partial positive charge, we expect that the gold nanoparticles were in the same state during the reaction both in the calcined and reduced catalysts. Therefore, we believe that the slightly decreased reaction rate was caused by the less OH groups and adsorbed water on the surface of alumina in the freshly reduced state than on the calcined sample stored one day at ambient conditions before reaction. The decrease of the concentration of OH groups after the in situ heat treatment was well seen on the IR spectra (3750 – 2500 cm^{-1}, not shown). Promotion by water and hydroxyl

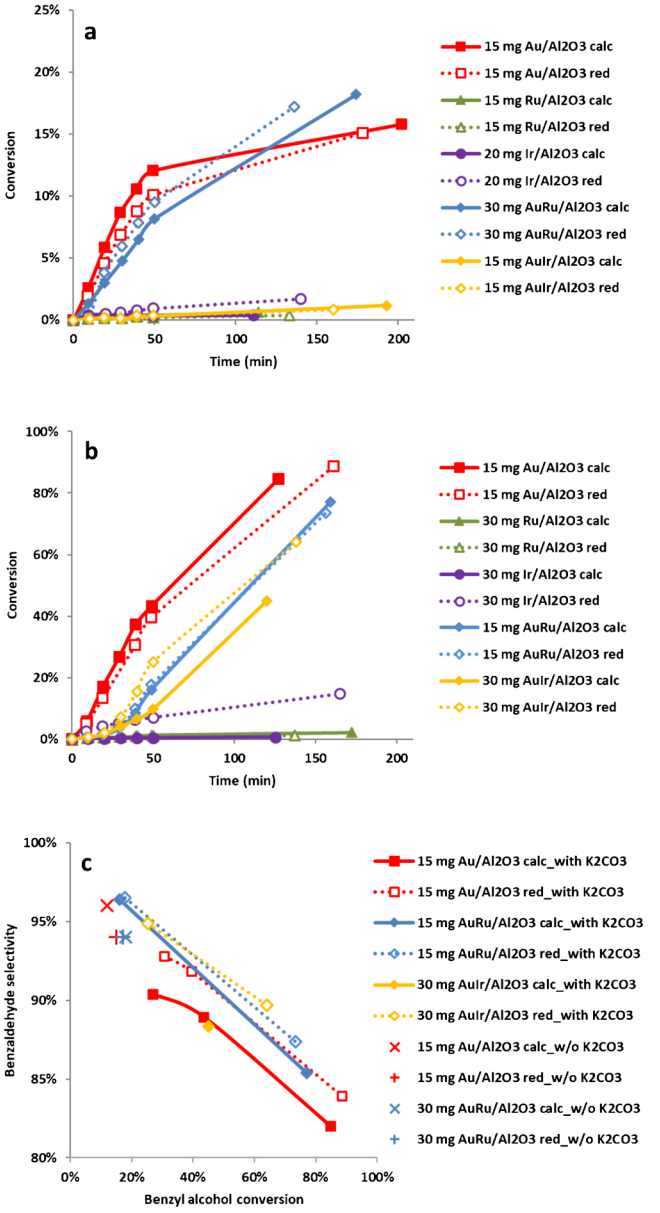

Fig. 8. Benzyl alcohol conversion curves of the calcined and reduced catalysts without added K_2CO_3 (a), and with added K_2CO_3 (b); benzaldehyde selectivity as a function of conversion (c).

groups was observed in both CO and alcohol oxidation on gold [62]. However, in case of the calcined and reduced state of the bimetallic catalysts the role of the second metal and the topmost surface composition must be more dominant, than that of OH groups.

On **Ru/Al_2O_3** hardly any conversion was measured both in calcined and reduced states, that is partly due to the very low dispersion of RuO_2 and metallic Ru, which on the other hand are low activity states of ruthenium in alcohol oxidation according to the literature. For alumina supported highly dispersed $Ru(OH)_3$, that is regarded the most active form of ruthenium in alcohol oxidation, TOF: 78 $mol/h/mol_{Ru}$ was reported [28] in similar reaction conditions to our ones, but without base addition. A lower value (TOF ≈ 30 $mol/h/mol_{Ru}$) was measured at 80 °C for a ruthenium hydrated oxide supported on alumina catalyst [25]. **AuRu/Al_2O_3** was active in all cases and the conversion curves of its calcined and reduced states were very similar. Similarly, no much activity difference was observed between $Ru(OH)_x/CaZrO_2$ calcined and reduced at 300 °C in 1-phenylethanol oxidation [26]. Without K_2CO_3 the initial reaction rates were lower than in the case of Au/

Table 3
Comparison of the initial reaction rates in the benzyl alcohol oxidation and the relative amount of CO adsorbed on gold.

Catalysts	Initial reaction rate mmol/h/g_{cat}				Relative IR band intensity of CO adsorbed on Au		Initial reaction rate mol/h/mol_{metal}			
	without K_2CO_3		with K_2CO_3				without K_2CO_3		with K_2CO_3	
	Calc	Red	Calc	Red	Calc	Red	Calc	Red	Calc	Red
Au/Al_2O_3	34	26	102	87	1.00	0.87	373	284	1122	956
Ru/Al_2O_3	2	1	1	1	–	–	33	16	24	29
$AuRu/Al_2O_3$	9	11	73[a]	79[a]	0.07	0.07	113	130	885[a]	965[a]
Ir/Al_2O_3	1	2	1	11	–	–	8	11	3	58
$AuIr/Al_2O_3$	0	1	16[a]	51[a]	0.05	0.03	6	13	250[a]	791[a]

[a] After induction period.

Al_2O_3, but at 175-minute reaction reached a higher conversion (17 %). The ruthenium may be able to decrease the poisonous effect of the benzoic acid. With K_2CO_3 a 30-minute-long induction period appeared. After that the activity of $AuRu/Al_2O_3$ approached that of the monometallic gold sample (see Table 3). We think the ruthenium particles' surface was more contaminated, than the gold's one and slowly became accessible for benzyl alcohol substrate. Furthermore, the ruthenium covered most of the gold surface, thus it took more time for the reaction medium to wet the gold's surface too, and hence the accessibility of benzyl alcohol to the gold's surface was limited at the beginning.

The **Ir/Al_2O_3** (having about 2 and 4 times higher molar metal loading compared to Au/Al_2O_3 and Ru/Al_2O_3 catalysts) presented negligible conversion in calcined state, but on the reduced form in base free reaction it increased somewhat, in case of added base more increased conversions were measured. The reaction rate decreased with time in both latter cases, though the conversion was below 10 %. We think that during the reaction iridium reoxidized to some extent resulting in the activity decrease with time. The reaction rates were very low even though we used much higher amount of Ir compared to the other catalysts (see Fig. 8). The **$AuIr/Al_2O_3$** was active only in the presence of K_2CO_3 showing an induction period in both calcined and reduced states similarly to the $AuRu/Al_2O_3$, but lower specific activity was observed especially in calcined form than in case of the $AuRu/Al_2O_3$ (as well visible by comparison of the reaction rates in Table 3). The reduced form was more active as in case of monometallic Ir/Al_2O_3.

3.4. Effect of the second metal (Ru and Ir) on Au/Al_2O_3 in benzyl alcohol oxidation

Since the activity of the alumina supported monometallic Ru and Ir was negligible compared to that of the gold, for estimation of the second metal effect it is most reasonable to compare the initial reaction rates related to the accessible Au sites. The Au surface in $AuRu/Al_2O_3$ and $AuIr/Al_2O_3$ samples with Au concentrations half of that of Au/Al_2O_3 and larger sizes (mean $d \geq 3.7$ nm for Au-Ru and ≥ 5.0 nm for Au-Ir) than in Au/Al_2O_3 (about 2.0 nm) by all means were more than 3 and 4 times smaller, than in the monometallic Au/Al_2O_3 catalyst, respectively, if Au was not enriched on the surface of the bimetallic particles. Indeed, CO adsorption followed by DRIFT spectroscopy, STEM-EDS and in case of $AuRu/Al_2O_3$ also XPS results suggested the enrichment of Ir and Ru on the surface of the bimetallic particles further decreasing the concentration of surface Au atoms. On the contrary in reaction with base addition the specific activity of the $AuRu/Al_2O_3$ (both calcined and reduced) and the reduced $AuIr/Al_2O_3$ were only less than 1.5 and 2 times lower, respectively, than that of Au/Al_2O_3. These more than two times higher activities of these bimetallic samples related to surface Au atoms indicate the synergistic co-operation/interaction of Au with both Ru and Ir in the benzyl alcohol oxidation. The calcined $AuIr/Al_2O_3$ presented much lower activity, about 6 times lower one, than the calcined Au/Al_2O_3, so in this case the interaction of Au and Ir-oxide did not show such activity enhancement. However, the above estimation of the $Au_{surface}$ concentrations gave only an upper limit of those in the bimetallic samples, because we assumed the same Au/Ru or Au/Ir atomic ratio on the surface as in the bulk. However, the structural characterizations pointed to the surface enrichment of Ru and Ir over Au.

Measurement of the amount of adsorbed CO on Au sites (proportional with its IR band intensity) can give a guess for the availability of gold on the top surface, even though only the coordinatively unsaturated surface Au atoms (their proportion on the Au surface decreases with increasing size [63]) can adsorb CO. In the bimetallic $AuRu/Al_2O_3$ and $AuIr/Al_2O_3$ catalysts the CO adsorbed on Au were less than 10 and 5%, respectively, of that measured on Au/Al_2O_3 sample of the same amount. If we take into account the different particle sizes and the corresponding proportion of the low coordinated Au atoms on the Au surface (as calculated for Au nanoparticles in [63]), on the Au particles of 2.0 nm mean diameter in the Au/Al_2O_3 it is about 1.8 and 2 times higher, than on particles of 3.8 and 5.0 nm in Au-Ru and Au-Ir samples, respectively. So if the second metals cover the surface Au atoms of different coordination in the same extent or less the low coordinated ones, the surface Au atom concentration in Au-Ru and Au-Ir catalysts are less than 15 and 10 % of that in monometallic gold sample, respectively, as estimated by the CO adsorbed. However, their specific reaction rates measured in the reaction with base addition did not reduce as much, proportionally, but it was higher than 65 % of that of Au/Al_2O_3 in case of $AuRu/Al_2O_3$ in both calcined and reduced states, while 50 % in case of reduced and only 15 % in case of calcined $AuIr/Al_2O_3$. In base free conditions the specific reaction rate of $AuRu/Al_2O_3$ was larger than 25 % of that of Au/Al_2O_3, while $AuIr/Al_2O_3$ was practically inactive. The trace amount of benzoic acid contamination of benzyl alcohol substrate must have poisoned in large extent the low concentration surface Au sites. All these further support that there are significant synergistic interactions of Au-Ru and Au-Ir operating in the bimetallic catalysts, except in the calcined $AuIr/Al_2O_3$.

Nevertheless, we must be cautious with this inference, since it is questionable if the benzyl alcohol oxidation is such a structure sensitive reaction, which has in the $4-5$ nm gold particle size range much higher surface Au atom related activity than in the $2-3$ nm range. In the literature there is no consensus about particle size effect in benzyl alcohol oxidation on Au catalysts. More results show increasing TOF [64–66] with decreasing size, but also the Au particles of 7 nm mean diameter was reported as the most active in the 1.3–11.3 nm size range [67].

4. Conclusions

Bimetallic sol-derived alumina supported Au-Ru (Au/Ru = 57/43) and Au-Ir (Au/Ir = 77/23) catalysts were compared with the corresponding monometallic ones in calcined and subsequently reduced states in selective aerobic benzyl alcohol oxidation without and with addition of K_2CO_3 base. The monometallic gold catalyst contained somewhat smaller size particles (with 2.0 nm mean diameter) compared to the bimetallic ones (AuRu: 3.8 nm, AuIr: 5.0 nm), the sizes were

practically the same in the calcined and reduced states. Compared to these the average size of Ir/Al_2O_3 was smaller (0.6 and 1.5 nm in the calcined and subsequently reduced states), while that of Ru/Al_2O_3 was larger (11 nm). Though alloy formation could not be disclosed, the interaction of the metals was established in bimetallic particles in both bimetallic catalysts based on the following results. STEM-EDS evidenced the presence of bimetallic particles in the Au-Ru and Au-Ir parent sols, namely Au(-Ru) core-Ru shell/decoration and Au(-Ir) core with Ir enrichment/thin layer on its surface type particles. The DRIFT spectra of CO adsorbed on gold of bimetallic samples as compared to Au/Al_2O_3 in calcined states indicated larger electron deficiency of gold and its higher stability. On bimetallic samples the amount of CO adsorbed on gold largely decreased in both calcined and reduced states compared to Au/Al_2O_3. This is certainly due to the surface enrichment of the second metals over the bimetallic particles beside the lower gold loading and larger particle sizes. The higher stability of metallic Ir against oxidation and reducibility of Ru-oxide in bimetallic catalysts compared to the monometallic ones as deduced from TPR, XPS and CO-DRIFTS studies was also an indication of the interaction of gold with the second metals.

The monometallic Au/Al_2O_3 was the most active in all catalytic tests, while Ru/Al_2O_3 and Ir/Al_2O_3 had negligible activity, and the bimetallic samples were in between. In base-free reactions the deactivation at low conversions and the lower initial reaction rates than measured in presence of K_2CO_3 was explained by the poisoning effect of trace amount of benzoic acid. In the base added reaction the initial reaction rates related to the same molar metal content in case of both calcined and reduced Au-Ru and reduced Au-Ir catalysts approached that of Au/Al_2O_3. The synergistic effect of the two metals is suggested in these catalysts based on the much higher activity of monometallic gold compared to Ir and Ru, plus the Au loadings and the particle sizes/dispersions of the active phases (in case of bimetallic systems assuming even distribution of the two metals on the surface). It is even more expressed if also the enrichment of the second metal over gold on the surface of bimetallic particles is considered.

CRediT authorship contribution statement

G. Nagy: Writing - review & editing, Investigation. **T. Gál:** Formal analysis. **D.F. Srankó:** Investigation, Formal analysis. **G. Sáfrán:** Investigation, Formal analysis. **B. Maróti:** Investigation, Formal analysis. **I.E. Sajó:** Investigation, Formal analysis. **F.-P. Schmidt:** Investigation, Formal analysis. **A. Beck:** Conceptualization, Supervision.

Declaration of Competing Interest

The author declare that they have no competing financial interests or personal relationships that could have appeared to influence the work reported in this paper.

Acknowledgements

The support of the Hungarian Science and Research Fund (OTKA no. K-101854, K-101897, PD-121318), the project VEKOP-2.3.3-15-2016-00002 supported by the European Structural and Investment Funds, ESTEEM2 (FP7 project, no. 312483) and Professor F. Hofer (Institute for Electron Microscopy and Nanoanalysis, Graz University of Technology) is acknowledged. The authors are thankful to Dr. Anita Horváth and Miklós Németh (Centre for Energy Research) for her valuable remarks and his help in preparation of XPS Figures, respectively. The scheme was drawn with ACD/ChemSketch 2016.2.2 software.

Appendix A. Supplementary data

Supplementary material related to this article can be found, in the online version, at doi:https://doi.org/10.1016/j.mcat.2020.110917.

References

[1] M. Haruta, N. Yamada, T. Kobayashi, S. Iijima, Gold catalysts prepared by coprecipitation for low-temperature oxidation of hydrogen and of carbon monoxide, J. Catal. 115 (1989) 301–309, https://doi.org/10.1016/0021-9517(89)90034-1.
[2] V.V. Costa, M. Estrada, Y. Demidova, I. Prosvirin, V. Kriventsov, R.F. Cotta, S. Fuentes, A. Simakov, E.V. Gusevskaya, Gold nanoparticles supported on magnesium oxide as catalysts for the aerobic oxidation of alcohols under alkali-free conditions, J. Catal. 292 (2012) 148–156, https://doi.org/10.1016/j.jcat.2012.05.009.
[3] S. Martínez-González, A. Gómez-Avilés, O. Martynyuk, A. Pestryakov, N. Bogdanchikova, V.C. Corberán, Selective oxidation of 1-octanol over gold supported on mesoporous metal-modified HMS: the effect of the support, Catal. Today 227 (2014) 65–70, https://doi.org/10.1016/j.cattod.2013.10.035.
[4] A. Villa, N. Dimitratos, C.E. Chan-Thaw, C. Hammond, L. Prati, G.J. Hutchings, Glycerol oxidation using gold-containing catalysts, Acc. Chem. Res. 48 (2015) 1403–1412, https://doi.org/10.1021/ar500426g.
[5] A. Philip, J. Lihavainen, M. Keinänen, T.T. Pakkanen, Gold nanoparticle-decorated halloysite nanotubes – selective catalysts for benzyl alcohol oxidation, Appl. Clay Sci. 143 (2017) 80–88, https://doi.org/10.1016/j.clay.2017.03.015.
[6] T. Gao, T. Gao, W. Fang, Q. Cao, Base-free aerobic oxidation of 5-hydroxymethylfurfural to 2,5-furandicarboxylic acid in water by hydrotalcite-activated carbon composite supported gold catalyst, Mol. Catal. 439 (2017) 171–179, https://doi.org/10.1016/j.mcat.2017.06.034.
[7] T. Benko, A. Beck, O. Geszti, R. Katona, A. Tungler, K. Frey, L. Guczi, Z. Schay, Selective oxidation of glucose versus CO oxidation over supported gold catalysts, Appl. Catal. -Gen. 388 (2010) 31–36, https://doi.org/10.1016/j.apcata.2010.08.008.
[8] T. Benko, A. Beck, K. Frey, D.F. Sranko, O. Geszti, G. Safran, B. Maroti, Z. Schay, Bimetallic Ag-Au/SiO2 catalysts: formation, structure and synergistic activity in glucose oxidation, Appl. Catal. -Gen. 479 (2014) 103–111, https://doi.org/10.1016/j.apcata.2014.04.027.
[9] R. Wojcieszak, I.M. Cuccovia, M.A. Silva, L.M. Rossi, Selective oxidation of glucose to glucuronic acid by cesium-promoted gold nanoparticle catalyst, J. Mol. Catal. Chem. 422 (2016) 35–42, https://doi.org/10.1016/j.molcata.2016.02.008.
[10] S. Rautiainen, O. Simakova, H. Guo, A.-R. Leino, K. Kordás, D. Murzin, M. Leskelä, T. Repo, Solvent controlled catalysis: synthesis of aldehyde, acid or ester by selective oxidation of benzyl alcohol with gold nanoparticles on alumina, Appl. Catal. Gen. 485 (2014) 202–206, https://doi.org/10.1016/j.apcata.2014.08.003.
[11] N. Dimitratos, J.A. Lopez-Sanchez, D. Morgan, A. Carley, L. Prati, G.J. Hutchings, Solvent free liquid phase oxidation of benzyl alcohol using Au supported catalysts prepared using a sol immobilization technique, Catal. Today 122 (2007) 317–324, https://doi.org/10.1016/j.cattod.2007.01.002.
[12] G. Zhan, J. Huang, M. Du, D. Sun, I. Abdul-Rauf, W. Lin, Y. Hong, Q. Li, Liquid phase oxidation of benzyl alcohol to benzaldehyde with novel uncalcined bioreduction Au catalysts: high activity and durability, Chem. Eng. J. 187 (2012) 232–238, https://doi.org/10.1016/j.cej.2012.01.051.
[13] E. Skupien, R. Berger, V. Santos, J. Gascon, M. Makkee, M. Kreutzer, P. Kooyman, J. Moulijn, F. Kapteijn, Inhibition of a gold-based catalyst in benzyl alcohol oxidation: understanding and remediation, Catalysts 4 (2014) 89–115, https://doi.org/10.3390/catal4020089.
[14] J. Hu, L. Chen, K. Zhu, A. Suchopar, R. Richards, Aerobic oxidation of alcohols catalyzed by gold nano-particles confined in the walls of mesoporous silica, Catal. Today 122 (2007) 277–283, https://doi.org/10.1016/j.cattod.2007.01.012.
[15] G. Zhan, Y. Hong, V.T. Mbah, J. Huang, A.-R. Ibrahim, M. Du, Q. Li, Bimetallic Au–Pd/MgO as efficient catalysts for aerobic oxidation of benzyl alcohol: a green bio-reducing preparation method, Appl. Catal. Gen. 439–440 (2012) 179–186, https://doi.org/10.1016/j.apcata.2012.07.005.
[16] X. Huang, X. Wang, X. Wang, X. Wang, M. Tan, W. Ding, X. Lu, P123-stabilized Au–Ag alloy nanoparticles for kinetics of aerobic oxidation of benzyl alcohol in aqueous solution, J. Catal. 301 (2013) 217–226, https://doi.org/10.1016/j.jcat.2013.02.011.
[17] G. Nagy, T. Benkó, L. Borkó, T. Csay, A. Horváth, K. Frey, A. Beck, Bimetallic Au–Ag/SiO_2 catalysts: comparison in glucose, benzyl alcohol and CO oxidation reactions, React. Kinet. Mech. Catal. 115 (2015) 45–65, https://doi.org/10.1007/s11144-015-0835-2.
[18] O.A. Kirichenko, E.A. Redina, N.A. Davshan, I.V. Mishin, G.I. Kapustin, T.R. Brueva, L.M. Kustov, W. Li, C.H. Kim, Preparation of alumina-supported gold-ruthenium bimetallic catalysts by redox reactions and their activity in preferential CO oxidation, Appl. Catal. B Environ. 134–135 (2013) 123–129, https://doi.org/10.1016/j.apcatb.2012.12.039.
[19] F.-W. Chang, L.S. Roselin, T.-C. Ou, Hydrogen production by partial oxidation of methanol over bimetallic Au–Ru/Fe_2O_3 catalysts, Appl. Catal. Gen. 334 (2008) 147–155, https://doi.org/10.1016/j.apcata.2007.10.003.
[20] L.A. Calzada, S.E. Collins, C.W. Han, V. Ortalan, R. Zanella, Synergetic effect of bimetallic Au-Ru/TiO_2 catalysts for complete oxidation of methanol, Appl. Catal. B Environ. 207 (2017) 79–92, https://doi.org/10.1016/j.apcatb.2017.01.081.
[21] L. Prati, F. Porta, D. Wang, A. Villa, Ru modified Au catalysts for the selective oxidation of aliphatic alcohols, Catal. Sci. Technol. 1 (2011) 1624–1629, https://doi.org/10.1039/C1CY00218J.
[22] L.E. Chinchilla, C.M. Olmos, A. Villa, A. Carlsson, L. Prati, X. Chen, G. Blanco, J.J. Calvino, A.B. Hungria, Ru-modified Au catalysts supported on ceria-zirconia for the selective oxidation of glycerol, Catal. Today 253 (2015) 178–189, https://doi.

org/10.1016/j.cattod.2015.02.030.
[23] T. Mallat, A. Baiker, Oxidation of alcohols with molecular oxygen on solid catalysts, Chem. Rev. 104 (2004) 3037–3058, https://doi.org/10.1021/cr0200116.
[24] X. Yang, X. Wang, J. Qiu, Aerobic oxidation of alcohols over carbon nanotube-supported Ru catalysts assembled at the interfaces of emulsion droplets, Appl. Catal. Gen. 382 (2010) 131–137, https://doi.org/10.1016/j.apcata.2010.04.046.
[25] D.V. Bavykin, A.A. Lapkin, S.T. Kolaczkowski, P.K. Plucinski, Selective oxidation of alcohols in a continuous multifunctional reactor: ruthenium oxide catalysed oxidation of benzyl alcohol, Appl. Catal. Gen. 288 (2005) 175–184, https://doi.org/10.1016/j.apcata.2005.04.042.
[26] T. Yasu-eda, S. Kitamura, N. Ikenaga, T. Miyake, T. Suzuki, Selective oxidation of alcohols with molecular oxygen over Ru/CaO–ZrO_2 catalyst, J. Mol. Catal. Chem. 323 (2010) 7–15, https://doi.org/10.1016/j.molcata.2010.03.018.
[27] D. Jung, S. Lee, K. Na, RuO_2 supported NaY zeolite catalysts: effect of preparation methods on catalytic performance during aerobic oxidation of benzyl alcohol, Solid State Sci. 72 (2017) 150–155, https://doi.org/10.1016/j.solidstatesciences.2017.08.022.
[28] K. Yamaguchi, N. Mizuno, Scope, kinetics, and mechanistic aspects of aerobic oxidations catalyzed by ruthenium supported on alumina, Chem. - Eur. J. 9 (2003) 4353–4361, https://doi.org/10.1002/chem.200304916.
[29] N. Zhang, Y. Du, M. Yin, C. Guan, J. Feng, D. Li, Facile synthesis of supported $RuO_2{\cdot}xH_2O$ nanoparticles on Co–Al hydrotalcite for the catalytic oxidation of alcohol: effect of temperature pretreatment, RSC Adv. 6 (2016) 49588–49596, https://doi.org/10.1039/C6RA11167J.
[30] F. Nikaidou, H. Ushiyama, K. Yamaguchi, K. Yamashita, N. Mizuno, Theoretical and experimental studies on reaction mechanism for aerobic alcohol oxidation by supported ruthenium hydroxide catalysts, J. Phys. Chem. C 114 (2010) 10873–10880, https://doi.org/10.1021/jp101692j.
[31] J.B. Brazier, K. Hellgardt, K.K. (Mimi) Hii, Catalysis in flow: O_2 effect on the catalytic activity of $Ru(OH)_x$ /γ-Al_2O_3 during the aerobic oxidation of an alcohol, React. Chem. Eng. 2 (2017) 60–67, https://doi.org/10.1039/C6RE00208K.
[32] X. Bokhimi, R. Zanella, C. Angeles-Chavez, Rutile-supported Ir, Au, and Ir − Au catalysts for COoxidation, J. Phys. Chem. C 114 (2010) 14101–14109, https://doi.org/10.1021/jp103053e.
[33] A. Aguirre, C.E. Barrios, A. Aguilar-Tapia, R. Zanella, M.A. Baltanás, S.E. Collins, In-situ DRIFT study of Au–Ir/ceria catalysts: activity and stability for CO oxidation, Top. Catal. 59 (2016) 347–356, https://doi.org/10.1007/s11244-015-0425-6.
[34] A. Gómez-Cortés, G. Díaz, R. Zanella, H. Ramírez, P. Santiago, J.M. Saniger, Au − Ir/TiO_2 prepared by deposition precipitation with urea: improved activity and stability in CO oxidation, J. Phys. Chem. C 113 (2009) 9710–9720, https://doi.org/10.1021/jp810905n.
[35] A. Aguilar-Tapia, R. Zanella, C. Calers, C. Louis, L. Delannoy, Synergistic effects of Ir–Au/TiO_2 catalysts in the total oxidation of propene: influence of the activation conditions, Phys. Chem. Chem. Phys. 17 (2015) 28022–28032, https://doi.org/10.1039/C5CP00590F.
[36] L. Torrente-Murciano, B. Solsona, S. Agouram, R. Sanchis, J.M. López, T. García, R. Zanella, Low temperature total oxidation of toluene by bimetallic Au–Ir catalysts, Catal. Sci. Technol. 7 (2017) 2886–2896, https://doi.org/10.1039/C7CY00635G.
[37] J. Zhao, J. Ni, J. Xu, J. Xu, J. Cen, X. Li, Ir promotion of TiO_2 supported Au catalysts for selective hydrogenation of cinnamaldehyde, Catal. Commun. 54 (2014) 72–76, https://doi.org/10.1016/j.catcom.2014.05.012.
[38] R. Kawahara, K. Fujita, R. Yamaguchi, Cooperative catalysis by iridium complexes with a bipyridonate ligand: versatile dehydrogenative oxidation of alcohols and reversible dehydrogenation–hydrogenation between 2-Propanol and acetone, Angew. Chem. Int. Ed. 51 (2012) 12790–12794, https://doi.org/10.1002/anie.201206987.
[39] Z. Révay, T. Belgya, Principles of PGAA method, Handb. Prompt Gamma Act. Anal. Neutron Beams, Kluwer Academic Publishers, Dordrecht/Boston/New York, 2004, pp. 1–30.
[40] Zs. Révay, P. Kudějová, K. Kleszcz, S. Söllradl, C. Genreith, In-beam activation analysis facility at MLZ, Garching, Nucl. Instrum. Methods Phys. Res. Sect. Accel. Spectrometers Detect. Assoc. Equip. 799 (2015) 114–123, https://doi.org/10.1016/j.nima.2015.07.063.
[41] P.S.S. Kumar, A. Manivel, S. Anandan, M. Zhou, F. Grieser, M. Ashokkumar, Sonochemical synthesis and characterization of gold–ruthenium bimetallic nanoparticles, Colloids Surf. Physicochem. Eng. Asp. 356 (2010) 140–144, https://doi.org/10.1016/j.colsurfa.2010.01.004.
[42] K. Chakrapani, S. Sampath, The dual role of borohydride depending on reaction temperature: synthesis of iridium and iridium oxide, Chem. Commun. 51 (2015) 9690–9693, https://doi.org/10.1039/C5CC03182F.
[43] O.A. Kirichenko, E.A. Redina, N.A. Davshan, I.V. Mishin, G.I. Kapustin, T.R. Brueva, L.M. Kustov, W. Li, C.H. Kim, Preparation of alumina-supported gold-ruthenium bimetallic catalysts by redox reactions and their activity in preferential CO oxidation, Appl. Catal. B Environ. 134 (2013) 123–129, https://doi.org/10.1016/j.apcatb.2012.12.039.
[44] I.W. Bassi, F. Garbassi, G. Vlaic, A. Marzi, G.R. Tauszik, G. Cocco, S. Galvagno, G. Parravano, Bimetallic ruthenium-gold-on-magnesia catalysts: chemicophysical properties and catalytic activity, J. Catal. 64 (1980) 405–416, https://doi.org/10.1016/0021-9517(80)90513-8.
[45] S. Galvagno, Bimetallic Ru-Au catalysts: effect of the support, J. Catal. 69 (1981) 283–291, https://doi.org/10.1016/0021-9517(81)90165-2.
[46] Q. Zhang, K. Kusada, D. Wu, N. Ogiwara, T. Yamamoto, T. Toriyama, S. Matsumura, S. Kawaguchi, Y. Kubota, T. Honma, H. Kitagawa, Solid-solution alloy nanoparticles of a combination of immiscible Au and Ru with a large gap of reduction potential and their enhanced oxygen evolution reaction performance, Chem. Sci. 10 (2019) 5133–5137, https://doi.org/10.1039/C9SC00496C.
[47] C.W. Han, P. Majumdar, E.E. Marinero, A. Aguilar-Tapia, R. Zanella, J. Greeley, V. Ortalan, Highly stable bimetallic AuIr/TiO_2 catalyst: physical origins of the intrinsic high stability against sintering, Nano Lett. 15 (2015) 8141–8147, https://doi.org/10.1021/acs.nanolett.5b03585.
[48] Z. Xiao, X. Jiang, B. Li, X. Liu, X. Huang, Y. Zhang, Q. Ren, J. Luo, Z. Qin, J. Hu, Hydrous RuO_2 nanoparticles as an efficient NIR-light induced photothermal agent for ablation of cancer cells in vitro and in vivo, Nanoscale 7 (2015) 11962–11970, https://doi.org/10.1039/C5NR00965K.
[49] F.A. Frame, T.K. Townsend, R.L. Chamousis, E.M. Sabio, Th. Dittrich, N.D. Browning, F.E. Osterloh, Photocatalytic water oxidation with nonsensitized IrO_2 nanocrystals under visible and UV light, J. Am. Chem. Soc. 133 (2011) 7264–7267, https://doi.org/10.1021/ja200144w.
[50] S. Kundu, H. Liang, Shape-selective formation and characterization of catalytically active iridium nanoparticles, J. Colloid Interface Sci. 354 (2011) 597–606, https://doi.org/10.1016/j.jcis.2010.11.032.
[51] X. Hong, B. Li, Y. Wang, J. Lu, G. Hu, M. Luo, Stable Ir/SiO2 catalyst for selective hydrogenation of crotonaldehyde, Appl. Surf. Sci. 270 (2013) 388–394, https://doi.org/10.1016/j.apsusc.2013.01.035.
[52] C. Carnevillier, F. Epron, P. Marecot, Controlled preparation and characterization of plurimetallic Pt–Sn and Pt–Ir–Sn/Al_2O_3 reforming catalysts, Appl. Catal. Gen. 275 (2004) 25–33, https://doi.org/10.1016/j.apcata.2004.07.015.
[53] E. Pachatouridou, E. Papista, E.F. Iliopoulou, A. Delimitis, G. Goula, I.V. Yentekakis, G.E. Marnellos, M. Konsolakis, Nitrous oxide decomposition over Al_2O_3 supported noble metals (Pt, Pd, Ir): effect of metal loading and feed composition, J. Environ. Chem. Eng. 3 (2015) 815–821, https://doi.org/10.1016/j.jece.2015.03.030.
[54] D.J. Morgan, Resolving ruthenium: XPS studies of common ruthenium materials, Surf. Interface Anal. 47 (2015) 1072–1079, https://doi.org/10.1002/sia.5852.
[55] K. Chakarova, M. Mihaylov, S. Ivanova, M.A. Centeno, K. Hadjiivanov, Well-defined negatively charged gold carbonyls on Au/SiO_2, J. Phys. Chem. C 115 (2011) 21273–21282, https://doi.org/10.1021/jp2070562.
[56] M. Mihaylov, H. Knözinger, K. Hadjiivanov, B.C. Gates, Characterization of the oxidation states of supported gold species by IR spectroscopy of adsorbed CO, Chem. Ing. Tech. 79 (2007) 795–806, https://doi.org/10.1002/cite.200700029.
[57] K. Hadjiivanov, J.-C. Lavalley, J. Lamotte, F. Maugé, J. Saint-Just, M. Che, FTIR study of CO interaction with Ru/TiO_2 catalysts, J. Catal. 176 (1998) 415–425, https://doi.org/10.1006/jcat.1998.2038.
[58] P. Gelin, G. Coudurier, Y.B. Taarit, C. Naccache, Formation of iridium carbonyl complex in NaY zeolite, J. Catal. 70 (1981) 32–40, https://doi.org/10.1016/0021-9517(81)90314-6.
[59] F. Solymosi, E. Novak, A. Molnar, Infrared spectroscopic study on carbon monoxide-induced structural changes of iridium on an alumina support, J. Phys. Chem. 94 (1990) 7250–7255, https://doi.org/10.1021/j100381a054.
[60] M. Mihaylov, E. Ivanova, F. Thibault-Starzyk, M. Daturi, L. Dimitrov, K. Hadjiivanov, New types of nonclassical iridium carbonyls formed in Ir-ZSM-5: a Fourier transform infrared spectroscopy investigation, J. Phys. Chem. B 110 (2006) 10383–10389, https://doi.org/10.1021/jp057128t.
[61] K. Patrícia, R. Castro, M. Aurélio, S. Garcia, W.C. de Abreu, S. Anderson, A. de Sousa, C. Verônica, R. de Moura, J. Cláudio, S. Costa, E.M. de Moura, Aerobic oxidation of benzyl alcohol on a strontium-based gold material: remarkable intrinsic basicity and reusable catalyst, Catalysts 8 (2018) 83, https://doi.org/10.3390/catal8020083.
[62] M.S. Ide, R.J. Davis, The important role of hydroxyl on oxidation catalysis by gold nanoparticles, Acc. Chem. Res. 47 (2014) 825–833, https://doi.org/10.1021/ar4001907.
[63] T.V.W. Janssens, B.S. Clausen, B. Hvolbæk, H. Falsig, C.H. Christensen, T. Bligaard, J.K. Nørskov, Insights into the reactivity of supported Au nanoparticles: combining theory and experiments, Top. Catal. 44 (2007) 15, https://doi.org/10.1007/s11244-007-0335-3.
[64] H. Liu, Y. Liu, Y. Li, Z. Tang, H. Jiang, Metal − organic framework supported gold nanoparticles as a highly active heterogeneous catalyst for aerobic oxidation of alcohols, J. Phys. Chem. C 114 (2010) 13362–13369, https://doi.org/10.1021/jp105666f.
[65] T. Mitsudome, A. Noujima, T. Mizugaki, K. Jitsukawa, K. Kaneda, Efficient aerobic oxidation of alcohols using a hydrotalcite-supported gold nanoparticle catalyst, Adv. Synth. Catal. 351 (2009) 1890–1896, https://doi.org/10.1002/adsc.200900239.
[66] H. Tsunoyama, H. Sakurai, T. Tsukuda, Size effect on the catalysis of gold clusters dispersed in water for aerobic oxidation of alcohol, Chem. Phys. Lett. 429 (2006) 528–532, https://doi.org/10.1016/j.cplett.2006.08.066.
[67] P. Haider, B. Kimmerle, F. Krumeich, W. Kleist, J.-D. Grunwaldt, A. Baiker, Gold-catalyzed aerobic oxidation of benzyl alcohol: effect of gold particle size on activity and selectivity in different solvents, Catal. Lett. 125 (2008) 169–176, https://doi.org/10.1007/s10562-008-9567-5.